

# Meta-Learning Based Domain Prior With Application to Optical-ISAR Image Translation

Huaizhang Liao<sup>ID</sup>, Jingyuan Xia<sup>ID</sup>, Zhixiong Yang<sup>ID</sup>, Fulin Pan, Zhen Liu<sup>ID</sup>, and Yongxiang Liu<sup>ID</sup>, Member, IEEE

**Abstract**—This paper focuses on generating Inverse Synthetic Aperture Radar (ISAR) images from optical images, in particular, for orbit space targets. ISAR images are widely applied in space target observation and classification tasks, whereas, limited to the expensive cost of ISAR sample collection, training deep learning-based ISAR image classifiers with insufficient samples and generating ISAR samples from emulation optical images via image translation techniques have attracted increasing attention. Image translation has highlighted significant success and popularity in computer vision, remote sensing and data generation societies. However, most of the existing methods are implemented under the discipline of extracting the explicit pixel-level features and do not perform effectively while entailing translation to domains with specific implicit features, such as ISAR image does. We propose a meta-learning based domain prior to implicit feature modelling and apply it to CycleGAN and UNIT models to realize effective translations between the ISAR and optical domains. Two representative implicit features, ISAR scattering distribution feature from the physical domain and the classification identifying feature from the task domain, are elaborately formulated with explicit modelling in statistic form. A meta-learning based training scheme is introduced to leverage the mutual knowledge of domain priors across different samples, and thus allows few-shot learning capacity with dramatically reduced training samples. Extensive simulations validate that the obtained ISAR images have better visible-authenticity and training-effectiveness than the existing image translation approaches on various synthetic datasets. Source codes are available at <https://github.com/XYLGroup/MLDP>.

**Index Terms**—Image translation, meta-learning, generative model, ISAR image processing.

## I. INTRODUCTION

DEEP learning has witnessed significant success in target classification [1], [2], such as, the face [3], vehicle

Manuscript received 16 June 2023; revised 8 August 2023; accepted 17 September 2023. Date of publication 22 September 2023; date of current version 12 August 2024. This work was supported in part by the National Natural Science Foundation of China under Project 62171448, Project 61921001, Project 62131020, and Project 62022091; and in part by the National Key Research and Development Program of China under Project 2021YFB100800. This article was recommended by Associate Editor L. Chiariglione. (*Huaizhang Liao and Jingyuan Xia contributed equally to this work.*) (*Corresponding author: Jingyuan Xia.*)

The authors are with the College of Electronic Engineering, National University of Defense Technology, Changsha 410073, China (e-mail: lhz17@nudt.edu.cn; j.xia10@nudt.edu.cn; yzx21@nudt.edu.cn; panfulin21@nudt.edu.cn; zhen\_liu@nudt.edu.cn; lyx\_bible@sina.com).

Color versions of one or more figures in this article are available at <https://doi.org/10.1109/TCSVT.2023.3318401>.

Digital Object Identifier 10.1109/TCSVT.2023.3318401

and pedestrian classification [4]. However, the performance of these deep-learning based approaches are bounded by the quantity and quality of the training samples, leading to limitations on real-world applications when lacking of sufficient training data. In particular, target classification for space targets [5], [6], [7], [8] has become increasingly crucial, with the revolutionary developments in aerospace society and the accompanying explosion of the number of orbital targets, such as the Starlink satellites and Tiangong orbital stations. The orbital environment and remote distance urge Inverse Synthetic Aperture Radar (ISAR), to become the major tool to obtain the observation data from orbital space targets. Although the ISAR images have the capacity of all-day and all-weather target observing, the number of available ISAR images is typically less-sufficient to satisfy deep training. This is because that the ISAR image collection is cumbersome, expensive, and even impossible in specific situations. In the contrast, the emulative optical samples of space targets can be obtained through synthetic methods in applications, which are ease of use in sample generation. In this instance, this paper tends to generate space target ISAR images from their optical counterparts to collect effective samples for training ISAR deep classifiers.

Image-to-image translation [9] is the most widely applied sample generation tool, which focuses on style and content shifting [10]. It typically learns the mapping between two optical domains that contain different modalities [11], [12], styles [13], [14], [15] or attributes [16], [17], [18], [19]. Most of the existing methods are implemented within the optical domain translation. Various deep neural networks in an adversarial framework, known as generative adversarial network (GAN)-based models [20], [21], [22], are proposed and substantiated great advances in applications. Nevertheless, the existing GAN-based models fail to utilize the implicit features that are underlying specific non-affine projection. This leads to a result that there is no guarantee on the translation performance between domains with considerable implicit discrepancy beyond pixel-level distribution, and the translation from the optical to ISAR domain is a representative case.

Differing from the optical images, ISAR images contain physical features in terms of scattering distribution, which vary with the outline, surface material, motion of the targets, and the detection angle of the radar. Moreover, the identifying features of the ISAR image that are contributed to the classification

accuracy may not be explicit and visible. This results in little application of the existing image translation technique to ISAR data augmentation. Specifically, there are three main reasons: (i) the physical domain feature is typically neglected when being processed by the optical image translation models; (ii) the existing image translation approaches mainly focus on pixel-level and structural content generation, without taking a task-specific factor, e.g., classification identifying features, into account; and (iii) the accessible number of training samples for space targets is typically insufficient in practical, while the existing generative models demand a large number of training data.

In this paper, we propose a meta-learning based domain prior (MLDP) framework for implicit feature representation and incorporate it with the existing image translation models. The proposed MLDP is elaborately formulated in a statistical form with two representative domain priors in this paper, while the primary concept of enrolling prior knowledge through task-driven and property-specific motivation is fundamental and beyond the studied domains. Recalling the aforementioned issues, domain-specific knowledge in terms of ISAR physical and classification task domains are incorporated as priors to guarantee rational ISAR generation. The proposed domain priors are learned in an unsupervised way with unpaired optical and ISAR samples through a meta-learning (ML) framework. Specifically, two consistencies of the physical scattering distribution features and classification identifying features between the ordinary and fabricated ISAR images are proposed to employ a representation learning on implicit features with explicit modeling. In contrast to the pixel-level feature extraction, a scale-invariant feature transform (SIFT) [23] based non-affine projection is applied to formulate the scattering distribution features in terms of density and intensity. Meanwhile, the classification identifying features are learned by a Kullback-Leibler divergence based measurement, which strives to ensure that the generated ISAR samples contribute to effective training on deep ISAR classifiers. These two domain-specific priors are leveraged by an alternative meta-learning phase. In this way, the mutual knowledge of scattering distribution and classification identifying features across different training samples are extracted to realize an effective and adaptive few-shot learning on space targets. In this way, the proposed MLDP model is a capacity of quickly training on a significantly reduced number of samples and enjoying promoting generalization capacity on different space targets. MLDP model is applicable to incorporate with the existing adversarial generative models, such as CycleGAN [14], [24], [25], [26], [27] and UNIT [28], [29], for image translation. For the CycleGAN model, we merge the two domain priors in the form of a cycle-consistency, and optimize the generators by minimizing the leveraged consistency losses among the translation between the optical and ISAR domains. For the UNIT model, the MLDP implicit feature learning is realized via constraining the latent space training procedure and then optimize the encoders and decoders through the meta-training phase.

Incorporating MLDP with generative models brings the following merits: (i) *Good model interpretability*. The proposed

MLDP explicitly formulates domain priors with elaborate modeling in statistic model, therefore, achieving a good interpretability and ease of enrolling prior knowledge. (ii) *Better utilization on implicit feature*. Differ from the pixel-level structural feature transfer, MLDP attains superior performance on retaining implicit features of ISAR images that are underlying non-affine deformation with respect to physical and task domain priors. (iii) *Few-shot learning capacity*. The MLDP follows a meta-learning strategy that provides the generator with the capacity of few-shot learning on limited training data. Hence, the required training samples are significantly reduced and better generalization capacity for unseen space target is attained. The main contributions are listed below:

- We propose a meta-learning based domain priors framework, named MLDP, that is the capacity of modelling the implicit features with non-affine deformation.
- The proposed MLDP is applicable to be incorporated with the existing generative models including CycleGAN and UNIT. For the first time, the MLDP-based models achieve an effective optical-to-ISAR image generation with vision-authentic and training-effective results.
- With meta-learning based mutual knowledge extraction across training samples, the incorporation of the MLDP achieves significantly better generalization capacity.

## II. RELATED WORKS AND PRELIMINARIES

### A. Image Translation Approaches

The existing image translation approaches can be approximately divided into two categories: image translation within the optical domain to transfer styles or contents, and translation between the optical and specific domains that has a considerable discrepancy.

1) *Optical Image Translation*: Generative models have been widely applied to achieve optical image translation in terms of style and content, which are typically implemented in an adversarial framework with variational generators including GAN-based and VAE-based models. In early studies, the majority of image translation approaches are implemented in a supervised way, in which sufficient paired samples are given for training. The conditional GAN (cGAN) [30] and its variant, e.g., pixel-to-pixel model [13], are known to be effective on style transform due to the conditional constraints on structural features [15], [31]. However, labelled paired training samples are extremely time-consuming and sometimes insufficient in reality. To reduce the data-dependency, studies on unsupervised image translation have gained considerable attentions in recent years. Specifically, CycleGAN [14], [24], [25], [26], [27], DualGAN [32] and DiscoGAN [33] propose a cycle-consistency-based adversarial framework, where pixel-level features are retained through an invertible mapping between the original and target domains. Meanwhile, UNIT [28], [29] establishes a VAE-based model to learn a latent space where the original and target domains share mutual distribution, and transforms specific image content through encoding-decoding operation in the learned latent space. MUNIT [18] further designs content and style latent spaces to indicate domain-specific and domain-sharing features, and achieves

a better generalization-ability on arbitrary style translation. More recent works tend to improve the model capacity of content understanding via the attention module. SA-MUNIT [29] and AGCycleGAN [24] incorporate attention blocks with the UNIT and CycleGAN, respectively, therefore achieving style transform on the selective area with respect to content segmentation.

2) *SAR/ISAR Image Translation*: More recently, attention has focused on the provision of image translation between the optical and the SAR/ISAR images [34], [35], [36], [37], [38], [39], [40]. For example, Hwang et al. [36] propose a structure similarity index measure (SSIM) loss-based CycleGAN to achieve a supervised transformation from the given SAR images to the remote sensing counterparts. Therefore, the mapping between the texture feature and scattering distribution is overlooked, resulting in less effective performance in generating detailed contents, such as farmland and forest. In [35], a cGAN-based SAR-to-optical translation is proposed to generate optical images for classification. However, there is no evaluation on the effectiveness of the generated images towards classification accuracy. Besides, Zhou et al. [37] propose an auto-encoder framework to generate aircraft ISAR images with varying rotations based on sufficient training on labelled ISAR samples. It directly utilizes pixel-level consistency to generate ISAR aircraft with paired training samples.

### B. Meta-Learning Based Training Scheme

Meta-learning [41], [42], [43], [44], [45], [46], [47] has been substantiated by its superior performance in solving few-shot learning tasks. Typically, meta-learning approaches are additive to the existing deep-learning models, which employ learning across different training samples and thus extract mutual knowledge to accelerate the training process [48]. In recent works, Sun et al. propose meta-transfer learning [49] to realize fast convergence for deep network models when only limited labelled training data are given. Similar work in [50] combines meta-learning with GAN to provide better generalization capacity on multi-target recognition tasks. It introduces a meta-learning based GAN model which optimizes model parameters underlying meta-losses across multiple training samples. Zhang et al. in [51] propose the MetaGAN, a conceptually simple and general framework, for the few-shot learning to augment the vanilla few-shot classification models with the ability to distinguish between the real and fake data. Reference [52] adapts two meta-learning algorithms, model-agnostic meta-learning (MAML) [53] and reptile [54], to GANs, learning an optimal weight initialization. Reference [52] achieves a rapid convergence on the new generation tasks during the fine-tuning process.

## III. META-LEARNING BASED DOMAIN PRIOR

### A. Implicit Domain Prior Modeling

Differing from the general structural features and contents in pixel-level elements, the domain priors are latent and non-affined, thereof, defined as implicit features. Let  $\mathcal{O}$  and  $\mathcal{I}$  denote the optical domain and ISAR domain, respectively. From the Bayesian perspective, an arbitrary generative model

$G$  learns to produce fake ISAR image from their optical counterpart, denoted by  $G(\phi_G, \mathcal{O})$  where  $\phi_G$  denotes the parameters of the generative model, with respect to maintaining the consistency of implicit feature with the original ISAR image  $\mathcal{I}$ , which is underlying the maximum a posterior (MAP) framework. Such MAP estimation is applied to each domain prior, along with the pixel-level image reconstruction objective in the following form

$$\max_{\phi_G} \log p(\mathcal{I}|G(\phi_G, \mathcal{O})) + \log \prod_{y=1}^Y p(\mathcal{F}_y(\mathcal{I})|\mathcal{F}_y(G(\phi_G, \mathcal{O}))), \quad (1)$$

where  $\mathcal{F}_y(\cdot)$  indicates the non-affine mapping between the implicit domain prior feature and the pixel-level image input, and  $Y$  is the number of domain priors. In (1), the first term denotes the pixel-level data reconstruction, and the second term represents the domain prior consistency on each implicit feature, which can be expressed as

$$\sum_{y=1}^Y \log p(\mathcal{F}_y(\mathcal{I})|\mathcal{F}_y(G(\phi_G, \mathcal{O}))). \quad (2)$$

In this paper, two different non-affine implicit features from ISAR physical domain (PD) and task-driven classification domain (CD) are introduced to improve the generative models and the corresponding non-affined mappings are demonstrated below, respectively.

1) *ISAR Physical Domain Prior*: The ISAR image is composed of scattering points, the distribution of which are varying with the motion, rotation, and surface reflectivity of the targets, therefore, leading to physical domain implicit features. Define  $\mathcal{F}_P$  as the mapping for ISAR physical domain prior, then we have

$$\max_{\phi_G} \log p(\mathcal{F}_P(\mathcal{I})|\mathcal{F}_P(G(\phi_G, \mathcal{O}))), \quad (3)$$

which demonstrates that the ISAR physical domain prior mapped from the ordinary ISAR image  $\mathcal{I}$  and the fake ISAR image  $G(\phi_G, \mathcal{O})$  should keep consistency.

In this paper, the mapping  $\mathcal{F}_P$  is achieved by a SIFT-based projection which extracts the largest scattering intensity with the precise coordinate, the greatest direction of intensity variation and the module of direction for the  $k^{th}$  scattering point in ISAR images, denoted by  $\hat{\mathbf{c}}^k, \theta^k$  and  $\mathcal{M}^k$ , respectively. Specifically, the formulations of  $\hat{\mathbf{c}}^k, \theta^k$  and  $\mathcal{M}^k$  are given by

$$\hat{\mathbf{c}}^k = \mathbf{c}^k - \frac{\partial^2 \mathcal{S}^{-1}}{\partial \mathbf{c}^2} \frac{\partial \mathcal{S}}{\partial \mathbf{c}}, \quad (4)$$

$$\theta^k = \arctan \frac{(\mathcal{L}(x^k, y^k + 1, \sigma^k) - \mathcal{L}(x^k, y^k - 1, \sigma^k))}{(\mathcal{L}(x^k + 1, y^k, \sigma^k) - \mathcal{L}(x^k - 1, y^k, \sigma^k))}, \quad (5)$$

where  $\mathcal{S}$  denotes the difference of Gaussian space,  $\mathbf{c}^k$  denotes the scattering point with the largest intensity among the surrounding points, the function  $\mathcal{L}(x^k, y^k, \sigma^k) = \mathcal{N}(x^k, y^k, \sigma^k) \otimes \mathcal{I}$ ,  $\mathcal{N}(x^k, y^k, \sigma^k)$  indicates a Gaussian distribution with scale factor  $\sigma^k$ . Define  $\mathbf{v}^k$  as the ISAR physical domain implicit feature vector extracted via the non-affine

mappings (4)-(6)((6), shown at the bottom of the page) at the  $k^{th}$  scattering point, which is expressed by

$$\mathbf{v}^k = [\hat{\mathbf{c}}^k, \theta^k, \mathcal{M}^k]^T, (k = 1, 2, \dots, K), \quad (7)$$

where  $T$  denotes the transposition and  $\hat{\mathbf{c}}^k$  denotes the precise coordinates of the extracted scattering point. Let  $\mathbf{V} = [\mathbf{v}^1, \mathbf{v}^2, \dots, \mathbf{v}^K]^T$  denote the ISAR physical domain implicit feature matrix for the whole ISAR image containing  $K$  scattering points, then we have

$$\mathcal{V} = \mathcal{F}_P(\mathbf{I}). \quad (8)$$

Recalling to (2), the general ISAR physical domain prior is formulated through the following Bayesian model

$$\max_{\phi_G} \log p(\mathcal{V}|\hat{\mathcal{V}}), \quad (9)$$

where the  $\hat{\mathcal{V}}$  denotes the implicit feature matrix for the fake ISAR images generated through  $\mathcal{F}_P(G(\phi_G, \mathbf{O}))$ . In this way, the implicit ISAR distribution and intensity features are represented in an explicit fashion recalling to aforementioned SIFT procedure and are convenient to be incorporated with the generative model in (1).

2) *Task-Driven Classification Domain Prior*: The classification tasks aim to distinguish the target categories on the basis of identifying features that contain differentiable content or unique component. The identifying features of space ISAR targets are implicit and typically obtained through dimension reduction operations. We define the implicit identifying features in ISAR images that contribute to classification accuracy as the task-driven classification domain prior, which should be taken into account with the generation process for better training-effectiveness. Let  $\mathcal{F}_C$  denote the mapping for classification domain prior, then the identifying features between the ordinary ISAR image  $\mathbf{I}$  and the fake ISAR image  $G(\phi_G, \mathbf{O})$  retain the consistency as follows

$$\max_{\phi_G} \log p(\mathcal{F}_C(\mathbf{I})|\mathcal{F}_C(G(\phi_G, \mathbf{O}))). \quad (10)$$

In conventional methods, the classification domain prior  $\mathcal{F}_C$  has no explicit formulation and is typically modelled by deep-learning-based models, which embedded the target identifying features within the network parameters. In this work, we Let  $\phi_C$  denote the parameters of a deep classifier  $C$ ,  $\{\mathbf{I}^1, \mathbf{I}^2, \dots, \mathbf{I}^M\}$  is the training dataset with  $M$  samples and category labels  $\mathbf{l}^1, \mathbf{l}^2, \dots, \mathbf{l}^M$ . Then the MAP estimation of the training process is formulated as follows

$$\max_{\phi_C} \sum_{m=1}^M \log p(\mathbf{l}^m|C(\phi_C, \mathbf{I}^m)). \quad (11)$$

As aforementioned, the identifying features are utilized implicitly within the parameters  $\phi_C$  throughout the training process, which distinguish the target type via learning on  $M$  number of samples. The performance of classifier  $C$ , which

is determined by the parameters  $\phi_C$ , thereby quantitatively measures the identifying features. In this paper, we adopt the KL-divergence to measure the classification performance between the ISAR training samples and the corresponding labels. Let  $\mathcal{D}(\cdot||\cdot)$  denote the KL divergence, the MAP estimation problem in (11) can be rewritten as

$$\min_{\phi_C} \sum_{m=1}^M \mathcal{D}(\mathbf{l}^m||C(\phi_C, \mathbf{I}^m)). \quad (12)$$

In this instance, the implicit classification domain prior mapping is modelled with a quantitative measurement through the KL-divergence, revealing the level of the class separability of the identifying feature that is obtained through  $\phi_C$  with taking as input an arbitrary ISAR image  $\mathbf{I}$  as follows,

$$\mathcal{F}_C(\mathbf{I}) \propto \mathcal{D}(\mathbf{l}||C(\phi_C, \mathbf{I})) = \mathbb{E} \left[ \log \frac{\mathbf{l}}{C(\phi_C, \mathbf{I})} \right]. \quad (13)$$

(13) reveals that, recalling the primary objective that generates ISAR images as effective training samples, the classification domain prior mapping  $\mathcal{F}_C$  is replaced by the KL-divergence on the ISAR image  $\mathbf{I}$  classified by pre-trained classifier  $C$  and the corresponding label  $\mathbf{l}$  to measure the identifying feature embedded with the parameters  $\phi_C$ . Then, on the basis of KL-divergence measurements, (10) can be reformulated explicitly as

$$\max_{\phi_G} \log p(\mathcal{D}(\mathbf{l}||C(\phi_C, \mathbf{I}))|\mathcal{D}(\mathbf{l}||C(\phi_C, G(\phi_G, \mathbf{O}))))). \quad (14)$$

In this way, the generated fake ISAR images are constrained to attain identifying feature consistency with the original counterparts in terms of the KL-divergence measurements with respect to a specific pre-trained classifier  $C$  with parameters  $\phi_C$ . Meanwhile, we note that the primary objective of this work tends to train an ISAR image generator  $G$  with parameters  $\phi_G$  for effective classifier training. Through (14), it is straightforward that the generated ISAR samples, determined by  $\phi_G$ , will be assigned to train the classifier, determined by  $\phi_C$ . Therefore, a task-driven invertible classification domain prior flow is realized between the generative model and the ISAR classifier to bridge the classification accuracy and the generation performance.

### B. Meta-Learning Based Domain Priors Learning

In this paper, a meta-learning based training scheme is established to learn the mutual knowledge of domain priors. Let  $t = 1, 2, \dots, T$  denote the index of the training samples and the  $\mathcal{L}_G^t$  denote the generic training loss of an arbitrary generative model  $G$  with the  $t^{th}$  training sample. Then the parameters  $\phi_G^t$  are optimized as

$$\phi_G^{t+1} \leftarrow \phi_G^t - \gamma_G \cdot \mathcal{R}(\nabla_{\phi_G^t} \mathcal{L}_G^t), \quad (15)$$

$$\mathcal{M}(x, y) = \sqrt{(\mathcal{L}(x^k + 1, y^k, \sigma^k) - \mathcal{L}(x^k - 1, y^k, \sigma^k))^2 + (\mathcal{L}(x^k, y^k + 1, \sigma^k) - \mathcal{L}(x^k, y^k - 1, \sigma^k))^2}, \quad (6)$$

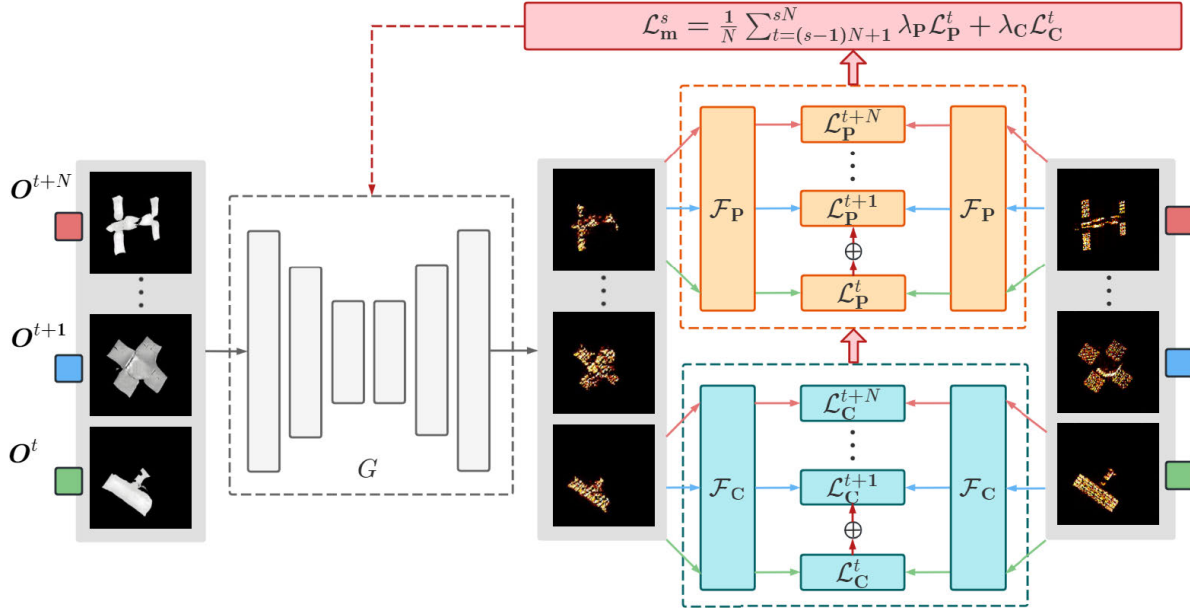


Fig. 1. The overview of the proposed MLDP framework for the optical to ISAR translation. The orange boxes represent the PD loss  $\mathcal{L}_P$  and SIFT mapping process  $\mathcal{F}_P$ , the cyan boxes indicate the CD loss  $\mathcal{L}_C$  and KL-divergence mapping procedure  $\mathcal{F}_C$ , and the red rectangle denotes the meta-loss  $\mathcal{L}_m$ .

where  $\gamma_G$  indicates the learning rate of the generic training stage and  $\mathcal{R}$  denotes an arbitrary optimizer, such as Adam or SGD.

Meanwhile, the ISAR physical and classification domain priors according to (9) and (14), can be formulated as additive losses that entail data (matrix/measurement) consistencies underlying each domain mapping for original/fake ISAR images. Define  $\mathcal{L}_P^t$  and  $\mathcal{L}_C^t$  as the losses of the ISAR physical domain and task-driven classification domain priors, respectively, and the formulations are given by

$$\mathcal{L}_P^t = -\log p(\mathcal{F}_P(\mathbf{I}^t) | \mathcal{F}_P(G(\phi_G^t, \mathbf{O}^t))), \quad (16)$$

$$\mathcal{L}_C^t = -\log p(\mathcal{F}_C(\mathbf{I}^t) | \mathcal{F}_C(G(\phi_G^t, \mathbf{O}^t))), \quad (17)$$

where the  $\mathbf{I}^t$  and  $\mathbf{O}^t$  denote the  $t^{th}$  ISAR and the optical training samples, respectively. The (16) and (17) describe the domain-specific feature consistencies between the real and fake ISAR images in terms of these two domains. Recalling the feature matrix of the scattering points in (9) and the KL-divergence measurement in (14), the general loss functions are given as follows

$$\mathcal{L}_P^t = \|\mathbf{V}^t - \hat{\mathbf{V}}^t\|_F^2, \quad (18)$$

$$\mathcal{L}_C^t = |\mathcal{D}(I||C(\phi_C, I^t)) - \mathcal{D}(I||C(\phi_C, G(\phi_G, O^t)))|. \quad (19)$$

As aforementioned in Section I, the available space target ISAR images are limited, while the domain priors learning are less straightforward than the contents and explicit features within ISAR samples. It is difficult to realize effective domain priors learning in the generic training scheme. In this stage, to address the issue of lacking sufficient training samples for domain priors learning, a meta-learning based strategy is proposed. A meta-loss  $\mathcal{L}_m$  across different samples on the  $\mathcal{L}_P^t$  and  $\mathcal{L}_C^t$  is proposed to optimize the generator  $G$ . Let  $s = 1, 2, \dots, T/N$  denote the meta-update index, where  $T$  is the maximum number of the training samples,  $N$  is the update

interval, and  $\mathcal{S} = \{N, 2N, \dots, T\}$  denote the set of update iteration index. The meta-learning based parameters update periodically executes when  $t \in \mathcal{S}$  which is given by

$$\mathcal{L}_m^s = \frac{1}{N} \sum_{t=(s-1)N+1}^{sN} \lambda_P \mathcal{L}_P^t + \lambda_C \mathcal{L}_C^t, \quad (20)$$

where  $\lambda_P$  and  $\lambda_C$  denote the weight parameters of the two domain priors losses, respectively. In this way, the mutual knowledge of the scattering distribution features and classification identifying feature measurements across different training samples are learned and leveraged to provide a few-shot learning capacity on the generative model  $G$ . The corresponding parameters update is given below

$$\phi_G^{s+1} \leftarrow \phi_G^s - \gamma_G \cdot \mathcal{R}(\nabla_{\phi_G^s} \mathcal{L}_m^s). \quad (21)$$

The proposed MLDP training scheme can be easily incorporated with the generic model training in the way of additive losses referring to (20). We note that, differ from the generic model training that minimizes the loss of the data discrepancy for each sample, MLDP takes accumulated losses over samples. Therefore, the objective of this meta-learning strategy no longer strives to minimize individual discrepancy, instead, it learns to extract the mutual knowledge that brings better performance for the least discrepancy on a set of samples. This provides the generative model a stronger capacity of capturing implicit features in domain priors with limited samples. The MLDP is convenient to be incorporated with arbitrary generative models to endow them with the capacity of utilization on implicit features in non-affine mapping domains.

#### IV. INCORPORATING MLDP TO CYCLEGAN

##### A. Original CycleGAN

The generic CycleGAN-based image translation framework tends to learn two invertible translations between the original

and target domains via simultaneously training two GANs with respect to two cycle-consistencies for two domain transform chains, respectively. This paper studies the Optical-to-ISAR unpaired image translation that entails two domain transform chains, the ISAR-Optical-ISAR chain, denoted by  $\mathcal{I}\mathcal{O}\mathcal{I}$ , and the Optical-ISAR-Optical chain, denoted by  $\mathcal{O}\mathcal{I}\mathcal{O}$ , in CycleGAN framework. Let  $G_{\mathcal{I}\mathcal{O}}$  be the generator with parameters  $\phi_{\mathcal{I}\mathcal{O}}$  for ISAR-to-Optical translation and the  $G_{\mathcal{O}\mathcal{I}}$  denote the counterpart generator with parameters  $\phi_{\mathcal{O}\mathcal{I}}$  for Optical-to-ISAR translation. At the same time,  $D_{\mathcal{O}}$  and  $D_{\mathcal{I}}$  are the discriminators with parameters  $\phi_{\mathcal{O}}$  and  $\phi_{\mathcal{I}}$ , which distinguish the input and generated samples from generators  $G_{\mathcal{I}\mathcal{O}}$  and  $G_{\mathcal{O}\mathcal{I}}$ , respectively. The discriminators carry a binary classification to distinguish the original samples and the generated samples. Mathematically, at the  $t^{th}$  training step, the total loss function of CycleGAN is given by

$$\mathcal{L}_{\text{cyc}}^t = \mathcal{L}_{\mathcal{I}\mathcal{O}}^t + \mathcal{L}_{\mathcal{O}\mathcal{I}}^t + \lambda_{\text{con}} \mathcal{L}_{\text{con}}^t, \quad (22)$$

where  $\mathcal{L}_{\mathcal{I}\mathcal{O}}^t$  and  $\mathcal{L}_{\mathcal{O}\mathcal{I}}^t$  indicate the adversarial losses of the transformation between the optical domain and ISAR domain as follows,

$$\mathcal{L}_{\mathcal{I}\mathcal{O}}^t = \mathbb{E}_{\mathcal{O}}[\log D_{\mathcal{O}}(\mathbf{O}^t)] + \mathbb{E}_{\mathcal{I}}[\log(1 - D_{\mathcal{O}}(G_{\mathcal{I}\mathcal{O}}(\mathbf{I}^t)))], \quad (23)$$

$$\mathcal{L}_{\mathcal{O}\mathcal{I}}^t = \mathbb{E}_{\mathcal{I}}[\log D_{\mathcal{I}}(\mathbf{I}^t)] + \mathbb{E}_{\mathcal{O}}[\log(1 - D_{\mathcal{I}}(G_{\mathcal{O}\mathcal{I}}(\mathbf{O}^t)))], \quad (24)$$

and the third term in (22) denotes the cycle-consistency loss  $\mathcal{L}_{\text{con}}^t$  with weight parameter  $\lambda_{\text{con}}$ , which is formulated as

$$\begin{aligned} \mathcal{L}_{\text{con}}^t &= \mathbb{E}_{\mathcal{I}}[\|G_{\mathcal{O}\mathcal{I}}(G_{\mathcal{I}\mathcal{O}}(\mathbf{I}^t)) - \mathbf{I}^t\|_1] \\ &\quad + \mathbb{E}_{\mathcal{O}}[\|G_{\mathcal{I}\mathcal{O}}(G_{\mathcal{O}\mathcal{I}}(\mathbf{O}^t)) - \mathbf{O}^t\|_1], \end{aligned} \quad (25)$$

where the first term describes the expectation of the consistency within the ISAR-Optical-ISAR transformation chain, and the second term represents the counterpart consistency in Optical-ISAR-Optical chain. More details of the basis of the CycleGAN can be found in [14], [24], [55], [56], and [57].

However, implementing CycleGAN framework on the Optical-to-ISAR translation problem is non-trivial. On the one hand, unlike the optical images, the natural properties contain implicit features, such as scattering distribution and identifying features, beyond self-similarity and structural features. The current cycle-consistency constructed on pixel-level image content may not be able to learn these implicit features. On the other hand, due to the limited acquiring accesses, there is no plenty of training samples for CycleGAN training, while most of the existing models demand a large amount of training samples. The primary training strategy may not work effectively on the space target translation tasks with insufficient training samples.

### B. Proposed MLDP-CycleGAN

We propose to incorporate the MLDP with the CycleGAN framework, referring to MLDP-CycleGAN. On the basis of the cycle-consistency, the ISAR physical and task-driven classification domain priors, referring to (18) and (19), are formulated

as two cycle-consistencies losses in the following forms

$$\mathcal{L}_{\text{P,cyc}}^t = \|\mathcal{F}_{\text{P}}(\mathbf{I}^t) - \mathcal{F}_{\text{P}}(G_{\mathcal{O}\mathcal{I}}(G_{\mathcal{I}\mathcal{O}}(\mathbf{I}^t)))\|_F^2, \quad (26)$$

$$\mathcal{L}_{\text{C,cyc}}^t = |\mathcal{F}_{\text{C}}(\mathbf{I}^t) - \mathcal{F}_{\text{C}}(G_{\mathcal{O}\mathcal{I}}(G_{\mathcal{I}\mathcal{O}}(\mathbf{I}^t)))|. \quad (27)$$

In MLDP-CycleGAN, we optimize the generators  $G_{\mathcal{O}\mathcal{I}}$  and  $G_{\mathcal{I}\mathcal{O}}$  in chains  $\mathcal{I}\mathcal{O}\mathcal{I}$  and  $\mathcal{O}\mathcal{I}\mathcal{O}$  with respect to domain priors cycle-consistency losses (26) and (27) rather than only with the ordinary CycleGAN loss (22) that entails pixel-level consistency and adversarial performance. More specifically, in forward propagation, the meta-loss across  $N$  training samples is periodically computed based on (20) as follows

$$\mathcal{L}_{\text{m,cyc}}^s = \frac{1}{N} \sum_{t=(s-1)N+1}^{sN} \lambda_{\text{P,cyc}} \mathcal{L}_{\text{P,cyc}}^t + \lambda_{\text{C,cyc}} \mathcal{L}_{\text{C,cyc}}^t, \quad (28)$$

where  $\lambda_{\text{P,cyc}}$  and  $\lambda_{\text{C,cyc}}$  are the weight parameters. Therefore, the total objectives of the proposed MLDP-CycleGAN at  $t^{th}$  step are formulated as

$$\left\{ \begin{array}{l} \Theta^{t+1}, \Xi^{t+1} = \arg \min_{\Theta} \max_{\Xi} \mathcal{L}_{\text{cyc}}^t, \\ \Phi^{s+1} = \arg \min_{\Phi} \mathcal{L}_{\text{m,cyc}}^s, \end{array} \right. \quad (29)$$

$$\Phi^{s+1} = \arg \min_{\Phi} \mathcal{L}_{\text{m,cyc}}^s, \quad (30)$$

where  $\Theta^{t+1} = \{\phi_{G_{\mathcal{I}\mathcal{O}}}^{t+1}, \phi_{G_{\mathcal{O}\mathcal{I}}}^{t+1}\}$  denotes the parameters set of generators  $G_{\mathcal{O}\mathcal{I}}$ ,  $G_{\mathcal{I}\mathcal{O}}$ ,  $\Xi^{t+1} = \{\phi_{D_{\mathcal{I}}}^{t+1}, \phi_{D_{\mathcal{O}}}^{t+1}\}$  denotes the parameters set of discriminators  $D_{\mathcal{O}}$ ,  $D_{\mathcal{I}}$  and  $\Phi^{s+1} = \{\phi_{G_{\mathcal{I}\mathcal{O}}}^{s+1}, \phi_{G_{\mathcal{O}\mathcal{I}}}^{s+1}\}$  denotes the parameters of the generators optimized by meta-loss  $\mathcal{L}_{\text{m,cyc}}^s$  at  $s^{th}$  meta-update index.

In this instance, the training of MLDP-CycleGAN contains two stages: CycleGAN training and MLDP training. Then the CycleGAN training is given by

$$\Theta^{t+1} \leftarrow \Theta^t - \Gamma_{\text{cyc}} \cdot \mathcal{R}(\nabla_{\Theta^t} \mathcal{L}_{\text{cyc}}^t), \quad (31)$$

$$\Xi^{t+1} \leftarrow \Xi^t + \Upsilon_{\text{cyc}} \cdot \mathcal{R}(\nabla_{\Xi^t} \mathcal{L}_{\text{cyc}}^t), \quad (32)$$

where  $\Gamma_{\text{cyc}} = \{\gamma_{G_{\mathcal{I}\mathcal{O}}}, \gamma_{G_{\mathcal{O}\mathcal{I}}}\}$  denotes the set of learning rates of the generators, and  $\Upsilon_{\text{cyc}} = \{\gamma_{D_{\mathcal{I}}}, \gamma_{D_{\mathcal{O}}}\}$  denotes the set of learning rates for the corresponding discriminators. Meanwhile, the MLDP training carries extra back-propagation of meta-loss  $\mathcal{L}_{\text{m,cyc}}^s$  to optimize the generators  $G_{\mathcal{I}\mathcal{O}}$ ,  $G_{\mathcal{O}\mathcal{I}}$  with respect to (20), which is given by

$$\Phi^{s+1} \leftarrow \Phi^s - \Gamma_{\text{cyc}} \cdot \mathcal{R}(\nabla_{\Phi^s} \mathcal{L}_{\text{m,cyc}}^s). \quad (33)$$

According to equations (28) to (33), the MLDP-CycleGAN is optimized in a hierarchical framework. Specifically, the backbone CycleGAN retains an adversarial training with cycle-consistency to realize the pixel-level reconstruction for structural features and explicit contents, while the MLDP employs periodic meta-training on generators to learn the implicit ISAR scattering distribution and the identifying features. The framework of the proposed MLDP-CycleGAN is shown in Fig 2.

The overall MLDP-CycleGAN training process is given in Algorithm 1. Let  $E$  denote the total number of the training epochs,  $\hat{\mathbf{I}}^t$  denote the generated ISAR image through the ISAR-Optical-ISAR process and  $\hat{\mathbf{O}}^t$  denote the generated optical image through the Optical-ISAR-Optical process. In each epoch, the generic CycleGAN training is iteratively operated with respect to the training samples  $\mathbf{I}^t$  and  $\mathbf{O}^t$  at each

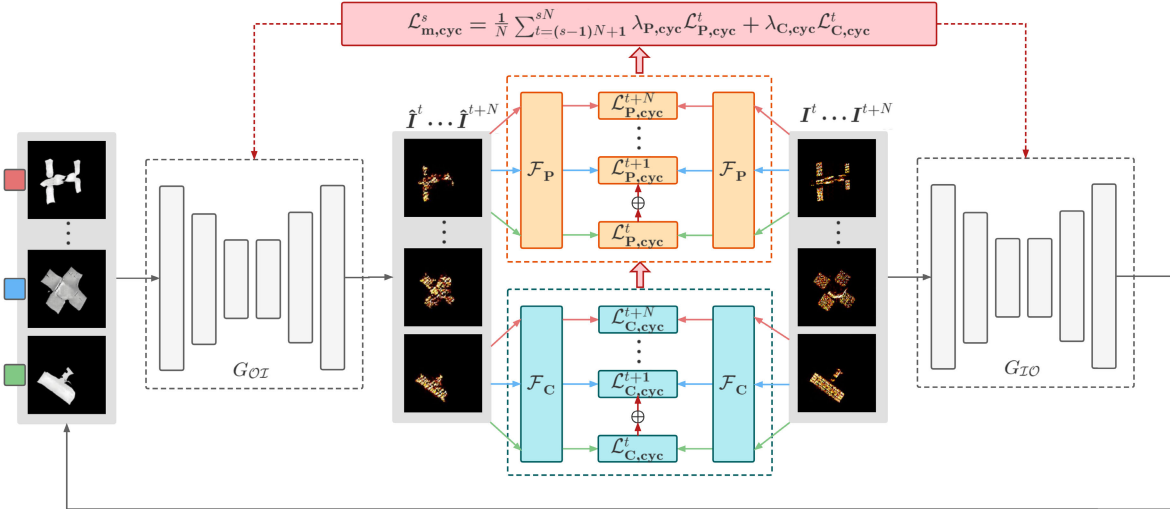


Fig. 2. The overview structure of the proposed MLDP-CycleGAN. The  $I^t \dots I^{t+N}$  denote the input ISAR samples, while the  $\hat{I}^t \dots \hat{I}^{t+N}$  denote synthesised ISAR space target samples based on the input optical images during the testing phase.

### Algorithm 1 MLDP-CycleGAN

```

1: Input: training samples:  $\{\mathbf{I}^t\}_{t=1}^T$ ,  $\{\mathbf{O}^t\}_{t=1}^T$ ; parameters:  $\lambda_{\text{con}}$ ,  $\lambda_{\text{P,cyc}}$ ,  $\lambda_{\text{C,cyc}}$ ; learning rates:  $\gamma_{G_{\mathcal{IO}}}$ ,  $\gamma_{G_{\mathcal{OI}}}$ ,  $\gamma_{D_{\mathcal{I}}}$ ,  $\gamma_{D_{\mathcal{O}}}$ ; meta-update index:  $s = 1$ 
2: while epoch  $\leftarrow 1, 2, \dots, E$  do
3:   while  $t \leftarrow 1, 2, \dots, T$  do
4:      $\hat{I}^t = G_{\mathcal{OI}}(G_{\mathcal{OI}}(\mathbf{I}^t))$ 
5:      $\hat{\mathbf{O}}^t = G_{\mathcal{OI}}(G_{\mathcal{OI}}(\mathbf{O}^t))$ 
6:      $\mathcal{L}_{\text{cyc}}^t = \mathcal{L}_{\mathcal{OI}}^t + \mathcal{L}_{\mathcal{OI}}^t + \lambda_{\text{con}} \mathcal{L}_{\text{con}}^t$ 
7:      $\Theta^{t+1} \leftarrow \Theta^t - \Gamma_{\text{cyc}} \cdot \mathcal{R}(\nabla_{\Theta^t} \mathcal{L}_{\text{cyc}}^t)$ 
8:      $\Xi^{t+1} \leftarrow \Xi^t + \Upsilon_{\text{cyc}} \cdot \mathcal{R}(\nabla_{\Xi^t} \mathcal{L}_{\text{cyc}}^t)$ 
9:     if  $t \in \mathcal{S}$  then
10:       $\Phi^s \leftarrow \Theta^{sN}$ 
11:       $\mathcal{L}_{\text{m,cyc}}^s = \frac{1}{N} \sum_{t=(s-1)N+1}^{sN} \lambda_{\text{P,cyc}} \mathcal{L}_{\text{P,cyc}}^t + \lambda_{\text{C,cyc}} \mathcal{L}_{\text{C,cyc}}^t$ 
12:       $\Phi^{s+1} \leftarrow \Phi^s - \Gamma_{\text{cyc}} \cdot \mathcal{R}(\nabla_{\Phi^s} \mathcal{L}_{\text{m,cyc}}^s)$ 
13:       $\Theta^{sN} \leftarrow \Phi^{s+1}$ 
14:       $s = s + 1$ 
15:    end if
16:  end while
17: end while

```

individual step, while the MLDP training is employed for every  $N$  steps across  $N$  pairs of training samples.

MLDP-CycleGAN embeds ISAR physical domain prior and classification domain prior into the network effectively by moving the domain prior consistency along the meta-learning training procedure over different ISAR samples, which enables few-shot capacity of quick learning on the implicit scattering distribution and identifying features. It is noteworthy that MLDP-CycleGAN does not require labelled and paired training data. It learns the implicit feature distribution between the optical and ISAR images in the way of mapping into physical and classification domains. Therefore, without massive training data and cumbersome data labeling demands, MLDP-CycleGAN can generate vision-authentic and training-effective

ISAR space target samples based on the input optical images during the testing phase.

## V. INCORPORATING MLDP TO UNIT

### A. Original UNIT

The common idea of the UNIT model is training two VAE-based generators to realize image translation between two domains via learning the domain-shared features in a latent space. This latent space is constructed by two weight-shared encoder-decoder networks for the bidirectional transform between optical and ISAR samples, respectively. For the Optical-to-ISAR image translation problem, UNIT framework is composed by two domain image encoders  $E_{\mathcal{I}}$ ,  $E_{\mathcal{O}}$  that encode the input samples into feature vectors in latent space, two domain image generators  $V_{\mathcal{I}}$ ,  $V_{\mathcal{O}}$  that decode feature vector to recover samples, and two domain adversarial discriminators  $B_{\mathcal{I}}$ ,  $B_{\mathcal{O}}$  that evaluate the generators' performance. At the  $t^{\text{th}}$  training step, the total loss of the UNIT model is formulated as follows

$$\mathcal{L}_{\text{uni}}^t = \mathcal{L}_{\text{ins}}^t + \mathcal{L}_{\text{acr}}^t + \mathcal{L}_{\text{adv}}^t, \quad (34)$$

where  $\mathcal{L}_{\text{ins}}^t$  is the domain-inside recovery loss,  $\mathcal{L}_{\text{acr}}^t$  is the domain-across cycle-reconstruction loss, and  $\mathcal{L}_{\text{adv}}^t$  is the adversarial loss. Specifically, let  $\mathbf{z}_{\mathcal{I}}^t$  and  $\mathbf{z}_{\mathcal{O}}^t$  denote the latent feature vectors, respectively,  $\mathcal{N}(\mathbf{z})$  is a zero-mean Gaussian distribution with random variable  $\mathbf{z}$ ,  $\hat{\mathbf{I}}_r^t$  and  $\hat{\mathbf{O}}_r^t$  are the recovered ISAR and optical images, respectively. Then the domain-inside loss is formulated as

$$\begin{aligned} \mathcal{L}_{\text{ins}}^t &= \lambda_1 \mathcal{D}(q_{\mathcal{I}}(\mathbf{z}_{\mathcal{I}}^t | \mathbf{I}^t) || \mathcal{N}(\mathbf{z})) - \lambda_2 \mathbb{E}_{\mathcal{I}}[\log p_{\mathcal{I}}(\hat{\mathbf{I}}_r^t | \mathbf{z}_{\mathcal{I}}^t)] \\ &\quad + \lambda_1 \mathcal{D}(q_{\mathcal{O}}(\mathbf{z}_{\mathcal{O}}^t | \mathbf{O}^t) || \mathcal{N}(\mathbf{z})) - \lambda_2 \mathbb{E}_{\mathcal{O}}[\log p_{\mathcal{O}}(\hat{\mathbf{O}}_r^t | \mathbf{z}_{\mathcal{O}}^t)], \end{aligned} \quad (35)$$

where  $q_{\mathcal{I}}$  and  $q_{\mathcal{O}}$  denote the latent feature distributions from ISAR and optical input, respectively,  $p_{\mathcal{I}}$  and  $p_{\mathcal{O}}$  are the Laplacian distribution describing the distributions of inverted reconstruction errors for ISAR and optical input, respectively. The KL divergence  $\mathcal{D}$  measures the discrepancy between

latent feature distribution and random Gaussian distribution with weight parameter  $\lambda_1$ . The expectation  $\mathbb{E}$  measures the reconstruction error with weight parameter  $\lambda_2$ .

The domain-across loss formulates external translation chains that bring additive divergence measurements on latent feature vectors, which is given as

$$\begin{aligned} \mathcal{L}_{\text{acr}}^t = & \lambda_3 [\mathcal{D}(q_{\mathcal{I}}(z_{\mathcal{I}}^t | \mathbf{I}^t) || \mathcal{N}(z)) + \mathcal{D}(q_{\mathcal{O}}(\hat{z}_{\mathcal{O},f}^t | V_{\mathcal{O}}(z_{\mathcal{I}}^t)) || \mathcal{N}(z))] \\ & + \lambda_3 [\mathcal{D}(q_{\mathcal{O}}(z_{\mathcal{O}}^t | \mathbf{O}^t) || \mathcal{N}(z)) + \mathcal{D}(q_{\mathcal{I}}(\hat{z}_{\mathcal{I},f}^t | V_{\mathcal{I}}(z_{\mathcal{O}}^t)) || \mathcal{N}(z))] \\ & - \lambda_4 \mathbb{E}_{\mathcal{I}}[\log(p_{\mathcal{I}}(\hat{\mathbf{I}}_r^t | \hat{z}_{\mathcal{O},f}^t))] - \lambda_4 \mathbb{E}_{\mathcal{O}}[\log(p_{\mathcal{O}}(\hat{\mathbf{O}}_f^t | \hat{z}_{\mathcal{I},f}^t))], \end{aligned} \quad (36)$$

where  $\hat{z}_{\mathcal{I},f}^t, \hat{z}_{\mathcal{O},f}^t$  denote the encoded latent feature vectors extracted from the fabricated ISAR and optical images,  $\hat{\mathbf{I}}_r^t$  and  $\hat{\mathbf{O}}_f^t$  denote the ISAR/optical image recovered from the generated optical/ISAR image, respectively,  $\lambda_3$  and  $\lambda_4$  are the weight parameters for KL-divergence and reconstruction expectation, respectively.

The adversarial loss  $\mathcal{L}_{\text{adv}}^t$  attains to evaluate the binary classification accuracy of the discriminators  $B_{\mathcal{I}}$  and  $B_{\mathcal{O}}$ , which follows the same formulations in (23) and (24).

Although UNIT model formulates a latent space for feature learning that is assumed to follow Gaussian distribution, the domain priors based implicit features will not emerge without incorporating expert knowledge as they involve different distributions. In this instance, the UNIT constructed latent space may not perform well on domain-across translation tasks that contain implicit features from domain priors.

### B. Proposed MLDP-UNIT

The instability of UNIT may come from the weak feature extraction of specific domain priors that are not explicitly embedded with the distribution of image pixels. In this case, the ordinary latent space feature encoding and decoding cannot capture implicit features in ISAR images, thus leading to less effective data generation. To alleviate the problem, we propose to incorporate the proposed MLDP into UNIT in order to constrain the latent space training procedure. We refer to this method as MLDP-UNIT and the total loss function of MLDP-UNIT is formulated

$$\mathcal{L}_{\text{MLDP,uni}}^t = \mathcal{L}_{\text{MLDP,ins}}^t + \mathcal{L}_{\text{MLDP,acr}}^t + \mathcal{L}_{\text{adv}}^t, \quad (37)$$

where  $\mathcal{L}_{\text{MLDP,ins}}^t$  and  $\mathcal{L}_{\text{MLDP,acr}}^t$  denote the domain-inside and domain-across losses with taking ISAR scattering distribution features and classification identifying features into account, respectively. In concrete, the  $\mathcal{L}_{\text{MLDP,ins}}^t$  is given in (38), shown

$$\begin{aligned} \mathcal{L}_{\text{MLDP,ins}}^t = & \lambda_1 \mathcal{D}(q_{\mathcal{I}}(z_{\mathcal{I}}^t | \mathbf{I}^t) || \mathcal{N}(z)) + \lambda_{\text{C,uni}} \mathcal{D}(\mathcal{F}_{\mathcal{C}}(z_{\mathcal{I}}^t) || \mathcal{F}_{\mathcal{C}}(\hat{z}_{\mathcal{I}}^t)) - \lambda_2 \mathbb{E}_{\mathcal{I}}[\log p_{\mathcal{I}}(\hat{\mathbf{I}}_r^t | z_{\mathcal{I}}^t)] + \lambda_{\text{P,uni}} \mathbb{E}_{\mathcal{I}}[\log p(\mathcal{F}_{\mathcal{P}}(\mathbf{I}^t) | \mathcal{F}_{\mathcal{P}}(\hat{\mathbf{I}}_r^t))] \\ & + \lambda_1 \mathcal{D}(q_{\mathcal{O}}(z_{\mathcal{O}}^t | \mathbf{O}^t) || \mathcal{N}(z)) - \lambda_2 \mathbb{E}_{\mathcal{O}}[\log p_{\mathcal{O}}(\hat{\mathbf{O}}_f^t | z_{\mathcal{O}}^t)]. \end{aligned} \quad (38)$$

$$\begin{aligned} \mathcal{L}_{\text{MLDP,acr}}^t = & \lambda_3 \mathcal{D}(q_{\mathcal{I}}(z_{\mathcal{I}}^t | \mathbf{I}^t) || \mathcal{N}(z)) + \lambda_3 \mathcal{D}(q_{\mathcal{O}}(\hat{z}_{\mathcal{O},f}^t | V_{\mathcal{O}}(z_{\mathcal{I}}^t)) || \mathcal{N}(z)) + \lambda_{\text{C,uni}} \mathcal{D}(\mathcal{F}_{\mathcal{C}}(z_{\mathcal{I}}^t) || \mathcal{F}_{\mathcal{C}}(\hat{z}_{\mathcal{I},f}^t)) \\ & - \lambda_4 \mathbb{E}_{\mathcal{I}}[\log(p_{\mathcal{I}}(\hat{\mathbf{I}}_r^t | \hat{z}_{\mathcal{O},f}^t))] + \lambda_{\text{P,uni}} \mathbb{E}_{\mathcal{I}}[\log p(\mathcal{F}_{\mathcal{P}}(\mathbf{I}^t) | \mathcal{F}_{\mathcal{P}}(\hat{\mathbf{I}}_f^t))] + \lambda_3 \mathcal{D}(q_{\mathcal{O}}(z_{\mathcal{O}}^t | \mathbf{O}^t) || \mathcal{N}(z)) \\ & + \lambda_3 \mathcal{D}(q_{\mathcal{I}}(\hat{z}_{\mathcal{I},f}^t | V_{\mathcal{I}}(z_{\mathcal{O}}^t)) || \mathcal{N}(z)) - \lambda_4 \mathbb{E}_{\mathcal{O}}[\log(p_{\mathcal{O}}(\hat{\mathbf{O}}_f^t | \hat{z}_{\mathcal{I},f}^t))]. \end{aligned} \quad (39)$$

at the bottom of the page, where  $\hat{z}_{\mathcal{I}}^t$  denotes the latent feature encoded from the recovered ISAR image  $\hat{\mathbf{I}}_r^t$ ,  $\lambda_{\text{C,uni}}$  and  $\lambda_{\text{P,uni}}$  represent the weight parameters of the classification domain prior and the ISAR physical domain prior, respectively. We note that the second term in (38) measures the classification discrepancy between the latent features  $z_{\mathcal{I}}^t$  and  $\hat{z}_{\mathcal{I}}^t$  instead of the input and output ISAR images, while the fourth term demonstrates the consistency of the scattering distribution features between the input ISAR sample  $\mathbf{I}^t$  and recovered ISAR image  $\hat{\mathbf{I}}_r^t$ , as the MLDP-CycleGAN does in cycle-consistency. Meanwhile,  $\mathcal{L}_{\text{MLDP,acr}}^t$  is formulated in (39), shown at the bottom of the page, where the third illustrates the similar classification discrepancy between the latent features  $z_{\mathcal{I}}^t$  and  $\hat{z}_{\mathcal{I}}^t$  and the fifth term indicates the consistency on ISAR scattering distribution features.

Different to the MLDP-CycleGAN, the proposed MLDP-UNIT leverages the classification identifying features on the basis of the ordinary latent space feature vector learning. In this way, the VAE-based encoder-decoder generator is optimized to ensure that the learned latent feature vectors are distinguishable in terms of classification accuracy. Let  $\mathcal{L}_{\text{DP,ins}}^t$  and  $\mathcal{L}_{\text{DP,acr}}^t$  denote the MLDP incorporated terms of domain priors in (38) and (39), respectively, then the incremental domain prior losses are given by

$$\begin{aligned} \mathcal{L}_{\text{DP,ins}}^t = & \lambda_{\text{C,uni}} \mathcal{D}(\mathcal{F}_{\mathcal{C}}(z_{\mathcal{I}}^t) || \mathcal{F}_{\mathcal{C}}(\hat{z}_{\mathcal{I}}^t)) \\ & + \lambda_{\text{P,uni}} \mathbb{E}_{\mathcal{I}}[\log p(\mathcal{F}_{\mathcal{P}}(\mathbf{I}^t) | \mathcal{F}_{\mathcal{P}}(\hat{\mathbf{I}}_r^t))], \end{aligned} \quad (40)$$

and

$$\begin{aligned} \mathcal{L}_{\text{DP,acr}}^t = & \lambda_{\text{C,uni}} \mathcal{D}(\mathcal{F}_{\mathcal{C}}(z_{\mathcal{I}}^t) || \mathcal{F}_{\mathcal{C}}(\hat{z}_{\mathcal{I},f}^t)) \\ & + \lambda_{\text{P,uni}} \mathbb{E}_{\mathcal{I}}[\log p(\mathcal{F}_{\mathcal{P}}(\mathbf{I}^t) | \mathcal{F}_{\mathcal{P}}(\hat{\mathbf{I}}_f^t))]. \end{aligned} \quad (41)$$

Then, according to (20), the meta-loss of the MLDP-UNIT domain priors  $\mathcal{L}_{\text{m,uni}}^t$  is formulated as

$$\mathcal{L}_{\text{m,uni}}^s = \frac{1}{N} \sum_{t=(s-1)N+1}^{sN} \mathcal{L}_{\text{DP,ins}}^t + \mathcal{L}_{\text{DP,acr}}^t. \quad (42)$$

Therefore, at the  $t^{\text{th}}$  iteration, the MLDP-UNIT carries a similar meta-learning based optimization strategy on trainable parameters in the following forms:

$$\left\{ \begin{array}{l} \Psi^{t+1}, \Pi^{t+1} = \arg \min_{\Psi} \max_{\Pi} \mathcal{L}_{\text{uni}}^t, \\ \Omega^{s+1} = \arg \min_{\Omega} \mathcal{L}_{\text{m,uni}}^s, \end{array} \right. \quad (43)$$

$$\left\{ \begin{array}{l} \Omega^{s+1} = \arg \min_{\Omega} \mathcal{L}_{\text{m,uni}}^s, \end{array} \right. \quad (44)$$

where  $\Psi^{t+1} = \{\phi_{E_{\mathcal{I}}}^{t+1}, \phi_{E_{\mathcal{O}}}^{t+1}, \phi_{V_{\mathcal{I}}}^{t+1}, \phi_{V_{\mathcal{O}}}^{t+1}\}$  is the set of parameters of encoders  $E_{\mathcal{I}}, E_{\mathcal{O}}$  and generators  $V_{\mathcal{I}}, V_{\mathcal{O}}$ ,

---


$$\begin{aligned} \mathcal{L}_{\text{MLDP,ins}}^t = & \lambda_1 \mathcal{D}(q_{\mathcal{I}}(z_{\mathcal{I}}^t | \mathbf{I}^t) || \mathcal{N}(z)) + \lambda_{\text{C,uni}} \mathcal{D}(\mathcal{F}_{\mathcal{C}}(z_{\mathcal{I}}^t) || \mathcal{F}_{\mathcal{C}}(\hat{z}_{\mathcal{I}}^t)) - \lambda_2 \mathbb{E}_{\mathcal{I}}[\log p_{\mathcal{I}}(\hat{\mathbf{I}}_r^t | z_{\mathcal{I}}^t)] + \lambda_{\text{P,uni}} \mathbb{E}_{\mathcal{I}}[\log p(\mathcal{F}_{\mathcal{P}}(\mathbf{I}^t) | \mathcal{F}_{\mathcal{P}}(\hat{\mathbf{I}}_r^t))] \\ & + \lambda_1 \mathcal{D}(q_{\mathcal{O}}(z_{\mathcal{O}}^t | \mathbf{O}^t) || \mathcal{N}(z)) - \lambda_2 \mathbb{E}_{\mathcal{O}}[\log p_{\mathcal{O}}(\hat{\mathbf{O}}_f^t | z_{\mathcal{O}}^t)]. \end{aligned} \quad (38)$$

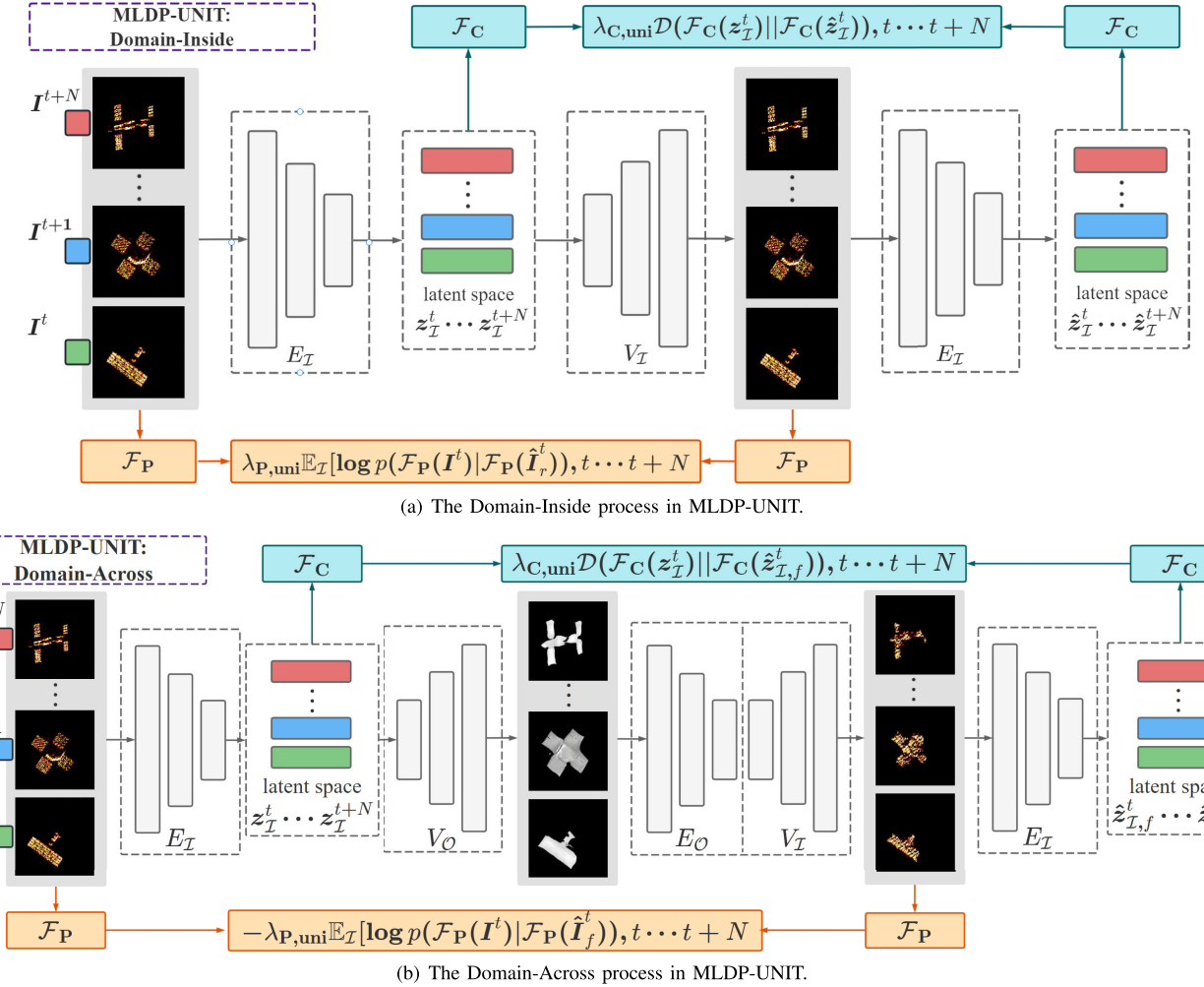


Fig. 3. The overview structure of the proposed MLDP-UNIT.

$\Pi^{t+1} = \{\phi_{B_I}^{t+1}, \phi_{B_O}^{t+1}\}$  is set of parameters of discriminators  $B_I, B_O$ , and  $\Omega^{s+1} = \{\phi_{E_I}^{s+1}, \phi_{E_O}^{s+1}, \phi_{V_I}^{s+1}, \phi_{V_O}^{s+1}\}$  denotes the set of parameters that are meta-optimized through  $\mathcal{L}_{m,uni}^s$  at each meta-update index  $s^{th}$ . The optimization phase in (43) refers to the generic UNIT training which is expressed as

$$\Psi^{t+1} \leftarrow \Psi^t - \Gamma_{uni} \cdot \mathcal{R}(\nabla_{\Psi^t} \mathcal{L}_{uni}^t), \quad (45)$$

$$\Pi^{t+1} \leftarrow \Pi^t + \Lambda_{uni} \cdot \mathcal{R}(\nabla_{\Pi^t} \mathcal{L}_{uni}^t), \quad (46)$$

where  $\Gamma_{uni} = \{\gamma_{E_I}, \gamma_{E_O}, \gamma_{V_I}, \gamma_{V_O}\}$  is a set of the learning rates of the encoders  $E_I, E_O$  and generators  $V_I, V_O$ , while  $\Lambda_{uni} = \{\gamma_{B_I}, \gamma_{B_O}\}$  denotes the set of learning rates of the discriminators  $B_I, B_O$ . Meanwhile, (44) reveals that the encoder and decoder networks  $E_I, E_O$  and  $V_I, V_O$  are further optimized with respect to the meta-loss across different samples, which is given by

$$\Omega^{s+1} \leftarrow \Omega^s - \Gamma_{uni} \cdot \mathcal{R}(\nabla_{\Omega^s} \mathcal{L}_{m,uni}^s). \quad (47)$$

The overall algorithm of the proposed MLDP-UNIT is demonstrated in Algorithm 2. In each epoch, the generic UNIT training is applied to each individual sample, and the meta-training is employed for every  $N$  number of samples. In Fig. 3, the elaborated data flows among domain-inside and domain-across loops are schematically illustrated. It is explicitly that

the MLDP-UNIT generates both domain-inside and domain-across samples from the latent feature vectors and uses it to enroll the implicit classification identifying feature with the encoder-decoder training.

## VI. EXPERIMENTS

### A. Experimental Setup

1) *Data Preparation:* In this paper, two datasets, named SL857 and SL585 respectively, that contain the unpaired optical and ISAR space target images, are synthetically constructed to evaluate the performance of the proposed MLDP model, as well as providing an accessible domain-across data resource for the image translation society. The SL857 contains 857 pairs of 10 categories of satellites optical and ISAR images with unpaired azimuth angles, and the training/testing apportion is set to 685/172 pairs while all the samples are distributed from these 10 categories with different azimuth angles. Meanwhile, SL585 contains 585 pairs of 10 categories of satellite optical and ISAR images, taking 6 categories of 394 pairs as training samples and another 4 categories of 172 pairs as testing samples. We present examples from SL857 and SL585 in Fig. 4 and Fig. 5. The training and testing samples in SL857 belong to the same categories with

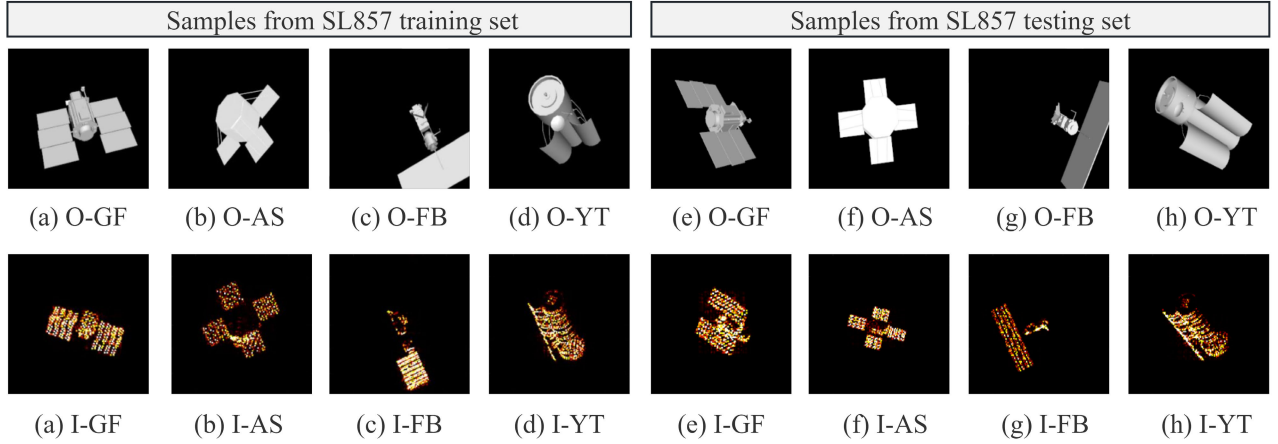


Fig. 4. The visualization of samples from SL857. The O denotes the optical images while I denotes the ISAR images. GF, AS FB and YT indicates the type of satellites. The azimuth angles of training samples are different from the angles of testing samples.

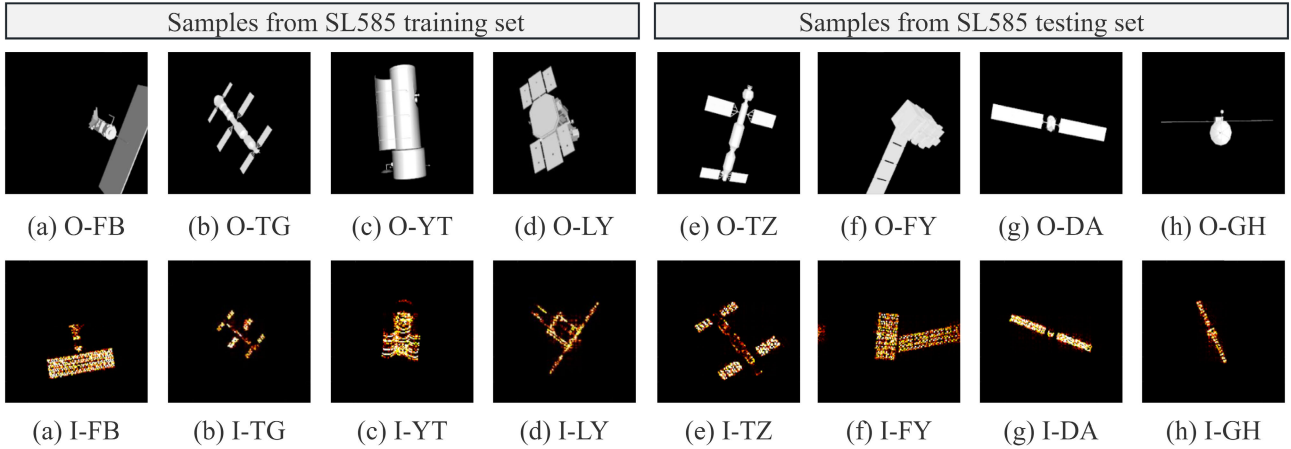


Fig. 5. The visualization of samples from SL585. In SL585, from left to right, the training set and testing set have different satellites, where training set has 6 categories of 394 pairs and testing set has 4 categories of 172.

significant difference on the azimuth angle and outlines, while the SL585 contains different training and testing samples. The optical images are obtained from the CAD software, while all the ISAR training samples are synthesized through the FEKO. The 10 categories of satellites contain AcrimSat, Dawn, Fengyun-3, Tiangong, Shenzhou and Tianzhou series.

2) *Implementation Details*: All simulations are carried on a single NVIDIA GeForce RTX 3090 GPU. We use Python 3.8 and Pytorch 1.9 frameworks for development. In MLDP-CycleGAN, the ordinary generative models follow the architectures in [14], which contains two stride-2 convolutions, 9 residual blocks and two  $\frac{1}{2}$ -strided convolutions, and the discriminators adopt  $70 \times 70$  PatchGANs [58]. The Adam [59] optimizer is applied with learning rates in set  $\Gamma_{\text{cyc}}$  and  $\Upsilon_{\text{cyc}}$  equal to  $8 \times 10^{-5}$ . The hyper-parameters  $\lambda_{\text{cyc}}$  is set to 5, and  $\lambda_{\text{P,cyc}}$  and  $\lambda_{\text{C,cyc}}$  are set to 1, and the meta-update interval  $N$  is set to 8. In MLDP-UNIT, we follow the VAE model in [28], which designs an encoder with 3 convolutional layers and 4 basic residual blocks and the corresponding decoder with 4 basic residual blocks and 3 transposed convolutional layers. The Adam optimizer is applied with learning rate  $10^{-4}$ . The hyper-parameters  $\lambda_0, \lambda_1, \lambda_2, \lambda_3, \lambda_4$  are set to 10, 0.1, 100, 0.1, 100, respectively, and  $\lambda_{\text{P,uni}}$  and  $\lambda_{\text{C,uni}}$  are set to 1 with the meta-update interval  $N = 8$ . Both the setting of the parameters

in MLDP-CycleGAN and MLDP-UNIT are refer to [14], [24], [28], [29], [55], [57], and [56].

Space target typically lack of ground truth data, therefore, the Inception Score (IS) [60], [61] is adopted to evaluate the clarify of the satellite target quantitatively. Meanwhile, the classification accuracy  $\mathcal{C}$  on testing datasets over 153 ISAR samples is calculated to evaluate the training-effectiveness via  $\mathcal{C} = \frac{1}{H} \sum_{i=1}^H T(l^i, C(\phi_C, I^i))$ , where  $H$  denotes the number of the testing samples,  $T$  determines whether the output of classifier  $C(\phi_C, I^i)$  is the same as the label  $l^i$ .

Five methods, including the ordinary CycleGAN [14] and UNIT [28], and three latest variants, including AGCycleGAN [24], MUNIT [18], and SA-MUNIT [29] are compared. Specifically, the vanilla CycleGAN and UNIT are evaluated as the baseline of the existing generative model performing on the optical to ISAR image translation task. AGCycleGAN incorporates an attention-based feature extraction module to achieve more adaptive transformation. Meanwhile, SA-MUNIT also integrates self-attention network with the UNIT model to endow stronger feature learning for image translation. Besides, MUNIT tends to learn domain-specific features across different domains, thus providing better generalization ability and adaptability on solving different style-transfer tasks.

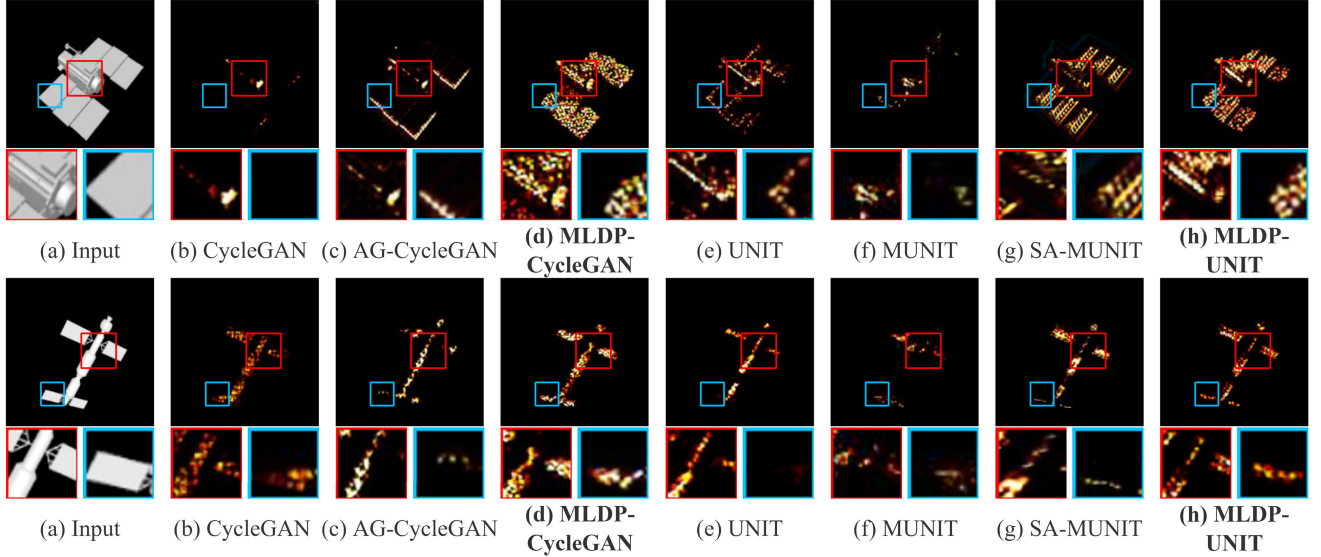


Fig. 6. The visual comparisons of the ISAR images generated by CycleGAN [14], AG-CycleGAN [24], UNIT [28], MUNIT [18], SA-MUNIT [29] and our methods. From top to down, the optical images are from SL857 and SL585.

### Algorithm 2 MLDP-UNIT

```

1: Input: training samples:  $\{\mathbf{I}^t\}_{t=1}^T$ ,  $\{\mathbf{O}^t\}_{t=1}^T$ ; parameters:  $\lambda_1$ ,
    $\lambda_2$ ,  $\lambda_3$ ,  $\lambda_4$ ,  $\lambda_{\text{P,uni}}$ ,  $\lambda_{\text{C,uni}}$ , learning rates:  $\gamma_{E_I}$ ,  $\gamma_{E_O}$ ,  $\gamma_{V_I}$ ,
    $\gamma_{V_O}$ ,  $\gamma_{B_I}$ ,  $\gamma_{B_O}$ ; meta-update index:  $s = 1$ 
2: while epoch  $\leftarrow 1, 2, \dots, E$  do
3:   while  $t \leftarrow 1, 2, \dots, T$  do
4:      $\hat{\mathbf{I}}_r^t = V_I(E_I(\mathbf{I}^t))$ 
5:      $\hat{\mathbf{O}}_r^t = V_O(E_O(\mathbf{O}^t))$ 
6:      $\hat{\mathbf{I}}_f^t = V_I(E_O(V_O(E_I(\mathbf{I}^t))))$ 
7:      $\hat{\mathbf{O}}_f^t = V_O(E_I(V_I(E_O(\mathbf{O}^t))))$ 
8:      $\mathcal{L}_{\text{uni}}^t = \mathcal{L}_{\text{ins}}^t + \mathcal{L}_{\text{acr}}^t + \mathcal{L}_{\text{adv}}^t$ 
9:      $\Psi^{t+1} \leftarrow \Psi^t - \Gamma_{\text{uni}} \cdot \mathcal{R}(\nabla_{\Psi^t} \mathcal{L}_{\text{uni}}^t)$ 
10:     $\Pi^{t+1} \leftarrow \Pi^t + \Lambda_{\text{uni}} \cdot \mathcal{R}(\nabla_{\Pi^t} \mathcal{L}_{\text{uni}}^t)$ 
11:    if  $t \in \mathcal{S}$  then
12:       $\Omega^s \leftarrow \Psi^{sN}$ 
13:       $\mathcal{L}_{\text{m,uni}}^s = \frac{1}{N} \sum_{t=(s-1)N+1}^{sN} \mathcal{L}_{\text{DP,ins}}^t + \mathcal{L}_{\text{DP,acr}}^t$ 
14:       $\Omega^{s+1} \leftarrow \Omega^s - \Gamma_{\text{uni}} \cdot \mathcal{R}(\nabla_{\Omega^s} \mathcal{L}_{\text{m,uni}}^s)$ 
15:       $\Psi^{sN} \leftarrow \Omega^{s+1}$ 
16:     $s = s + 1$ 
17:  end if
18: end while
19: end while

```

### B. Results and Analysis

1) *Image Translation Performance Comparisons:* In Fig. 6, we first show the visualization results of the seven methods. The first and second rows present the simulation results on SL857, and the third and fourth rows show the results on SL585. It is apparent from all the simulation results that the MLDP significantly improves the visible-authenticity of the generated ISAR images in terms of scattering distribution in image. Specifically, in SL857 results, the MLDP-CycleGAN achieves rational and dense ISAR scattering distribution while the vanilla CycleGAN and AGCycleGAN only translate the outline of the target when testing samples are with different

TABLE I  
THE IS RESULTS OF THE DIFFERENT TRANSLATION MODELS

Model	SL857	SL585
CycleGAN	1.70	1.57
AGCycleGAN	1.47	1.24
<b>MLDP-CycleGAN</b>	<b>2.41</b>	<b>2.38</b>
UNIT	1.73	1.56
MUNIT	1.54	1.32
SA-MUNIT	1.93	1.71
<b>MLDP-UNIT</b>	<b>2.56</b>	<b>2.49</b>

azimuth angles. At the same time, the existing UNIT models perform generally better results than CycleGAN models in terms of ISAR scattering distribution. This responses to the latent space learning that allows UNIT model being with better flexibility in learning non-affine features. However, the MLDP-UNIT still attains significantly better results than the compared UNIT models. When it comes to the results from SL585, in which the testing samples are different categories and unseen targets in training dataset, the existing generative models all present dramatic performance drop while the MLDP-based two models still retain good performance for rational ISAR scattering distributions. In Table I, the corresponding quantitative measurements on IS also validate the similar results. It is explicit that MLDP-based two generative models achieve a superior IS score than the existing CycleGAN and UNIT models.

The generalization-ability of the seven models are tested on two scenarios: unseen azimuth angles of the training samples in SL857 and unseen categories of satellites in SL585. The generated ISAR images and the corresponding IS results for these two challenging scenarios are presented in Fig. 7 and 8, respectively. Fig. 7 shows that only the MLDP-based two models keep the rational scattering distributions on all azimuth angles, while the others fail to learn the authentic scattering distribution features from training stage. The results in Fig. 8 report more significant performance discrepancy between the MLDP-based models and the existing generative models on unseen category simulation. In the third and fourth rows, the

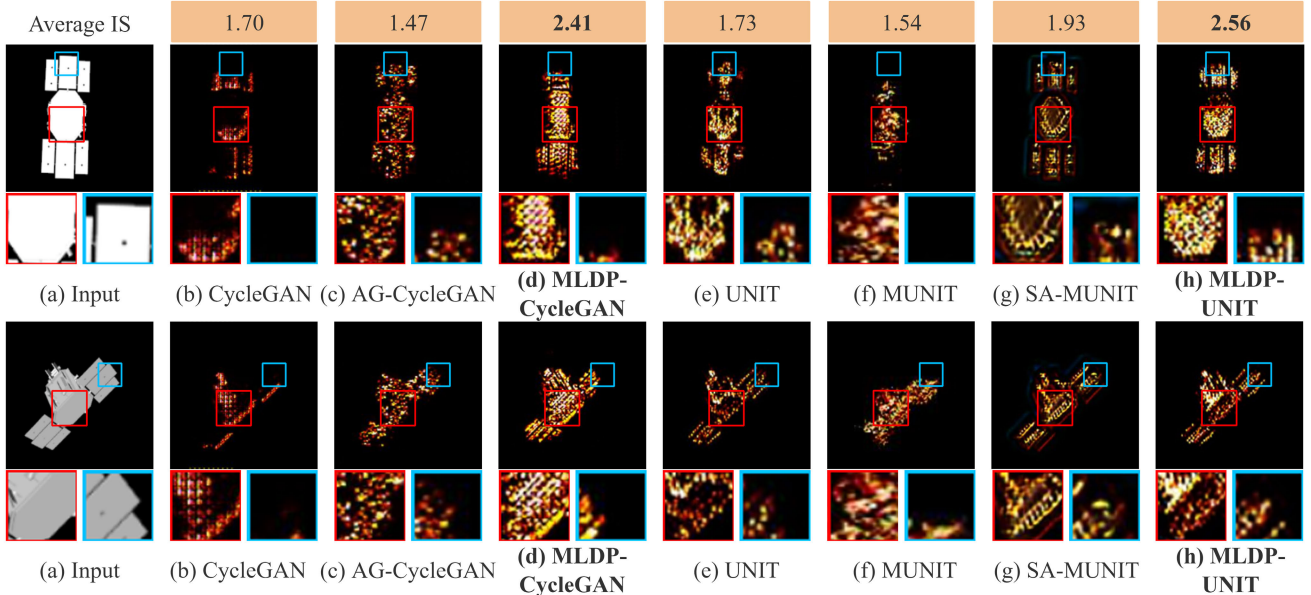


Fig. 7. The visual results of ISAR image generation in different azimuths from SL857. From top to down, the optical images are from the same satellite with different azimuths.

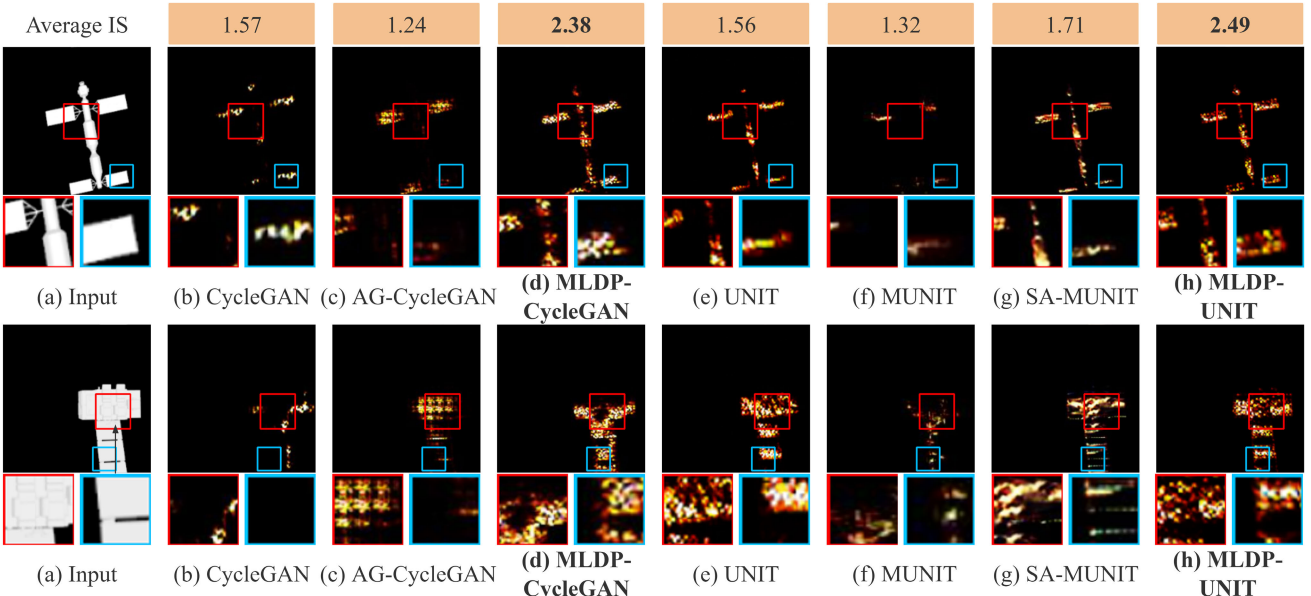


Fig. 8. The visual results of ISAR image generation in different categories from SL585. From top to down, the optical images are from different types of satellites.

TABLE II  
THE CLASSIFICATION ACCURACY OF CLASSIFIERS TRAINED BY DIFFERENT GENERATED SAMPLES

Classifier	Generated Samples	Original	CycleGAN	AGCycleGAN	MLDP-CycleGAN	UNIT	MUNIT	SA-MUNIT	MLDP-UNIT
VGG16	315	65.14%	59.60%	63.82%	<b>74.32%</b>	61.89%	60.01%	69.92%	<b>75.68%</b>
	630		61.35%	65.81%	<b>76.73%</b>	62.30%	63.02%	71.95%	<b>77.03%</b>
	1260		63.24%	66.88%	<b>79.05%</b>	63.11%	65.87%	72.52%	<b>79.43%</b>
	1890		64.12%	67.84%	<b>81.13%</b>	64.23%	68.13%	73.89%	<b>81.52%</b>
ResNet18	315	61.95%	52.43%	53.38%	<b>66.89%</b>	54.59%	53.70%	61.79%	<b>66.05%</b>
	630		54.32%	54.26%	<b>71.95%</b>	56.89%	55.72%	63.06%	<b>69.07%</b>
	1260		56.83%	55.35%	<b>75.00%</b>	54.12%	57.86%	64.86%	<b>71.27%</b>
	1890		58.29%	56.27%	<b>78.46%</b>	56.38%	60.04%	65.97%	<b>73.31%</b>

generated ISAR samples from the existing generative models are distorted, while the MLDP-CycleGAN and MLDP-UNIT generate the ISAR satellites with primary context and ISAR

scattering distribution features. The averaged IS measurements are given below the pictures, which also verify the superior generalization-ability of the MLDP framework.

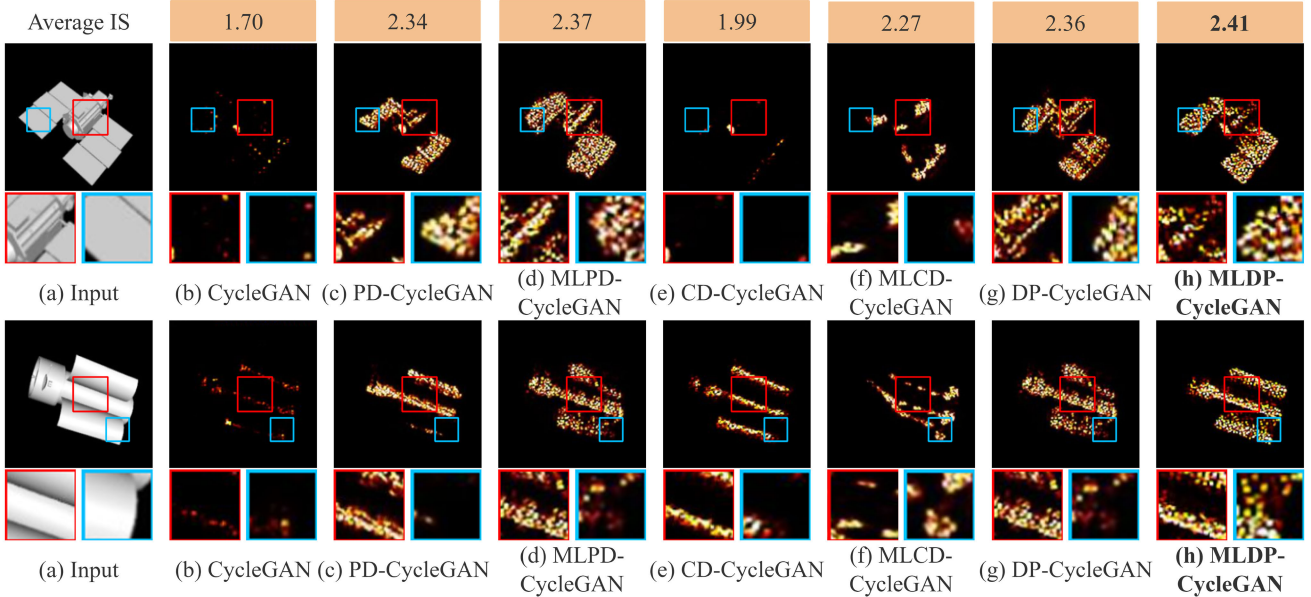


Fig. 9. The ablation results of the generated ISAR images from the vanilla CycleGAN to the proposed MLDP-CycleGAN framework.

TABLE III  
THE TRAINING-EFFECTIVENESS RESULTS OF THE CYCLEGAN FRAMEWORK

Classifier	Generated Samples	PD-CycleGAN	MLPD-CycleGAN	CD-CycleGAN	MLCD-CycleGAN	DP-CycleGAN	MLDP-CycleGAN
VGG16	315	67.97%	69.59%	70.97%	72.43%	72.97%	<b>74.32%</b>
	630	70.50%	71.62%	72.57%	74.19%	75.85%	<b>76.73%</b>
	1260	71.17%	74.32%	73.20%	75.51%	78.83%	<b>79.05%</b>
	1890	73.01%	76.13%	74.87%	76.84%	80.22%	<b>81.13%</b>
ResNet18	315	61.99%	62.70%	62.82%	64.73%	65.54%	<b>66.89%</b>
	630	62.61%	64.86%	65.58%	66.62%	67.57%	<b>71.95%</b>
	1260	64.59%	66.55%	67.34%	68.58%	69.95%	<b>75.00%</b>
	1890	65.89%	67.82%	68.27%	70.08%	70.84%	<b>78.46%</b>

2) *Training-Effectiveness for Deep Classifiers*: Table. II elaborates the training-effectiveness of the generated ISAR images with respect to two classifiers, VGG16 [62] and ResNet18 [63] that are trained by different sets of data. The “Original” denotes to the primary training dataset with 670 real ISAR samples, and the listed numbers refer to the additive generated samples mixed with the “Original” training dataset. In general, it can be seen that the MLDP-based two models successfully generate training-effective ISAR samples, surpassing all the tested existing models with significantly higher improvements on the classification accuracy. In details, with merely 315 generated ISAR samples, MLDP-CycleGAN improves the classification accuracy for approximately 9% for VGG16 and 5% for ResNet18, while MLDP-UNIT brings 10% and 5% improvements for VGG16 and ResNet18, respectively. With the incremental number of MLDP-based model generated ISAR samples enrolled, the classification accuracy rapidly increases to around 80% from the original 65% for VGG16, and the ResNet18 also enjoys around 16% increments on classification accuracy when 1890 generated ISAR samples are provided.

The most striking results to emerge from the Table. II are that except of the SA-MUNIT, rest of the existing models do not generate samples that contribute to the training of the deep classifiers. It is clear, the training with extra samples generated by the vanilla CycleGAN and UNIT models are detrimental to

TABLE IV  
THE ABLATION RESULTS OF IS

PD	CD	ML	Model	SL857	SL585
			CycleGAN	1.70	1.57
✓			PD-CycleGAN	2.34	2.17
✓	✓	✓	MLPD-CycleGAN	2.37	1.32
	✓		CD-CycleGAN	1.99	1.89
✓	✓	✓	MLCD-CycleGAN	2.27	2.25
✓	✓		DP-CycleGAN	2.36	2.26
✓	✓	✓	<b>MLDP-CycleGAN</b>	<b>2.41</b>	<b>2.38</b>
			UNIT	1.73	1.74
✓			PD-UNIT	2.32	2.12
✓	✓	✓	MLPD-UNIT	2.46	2.40
	✓		CD-UNIT	2.23	2.11
✓	✓	✓	MLCD-UNIT	2.39	2.35
✓	✓		DP-UNIT	2.50	2.35
✓	✓	✓	<b>MLDP-UNIT</b>	<b>2.56</b>	<b>2.48</b>

the classification accuracy, while AGCycleGAN and MUNIT also perform little contributions only with a large number of generated samples. This reveals that translation the optical image to ISAR samples underlying the learning on implicit features is nontrivial, and the proposed MLDP framework is with significance on data generation tasks.

3) *Ablation Experiments*: In this paper, two representative implicit features referring to physical domain (PD) and classification domain (CD) priors and a meta-learning (ML) scheme is proposed to realize the optical to ISAR translation.

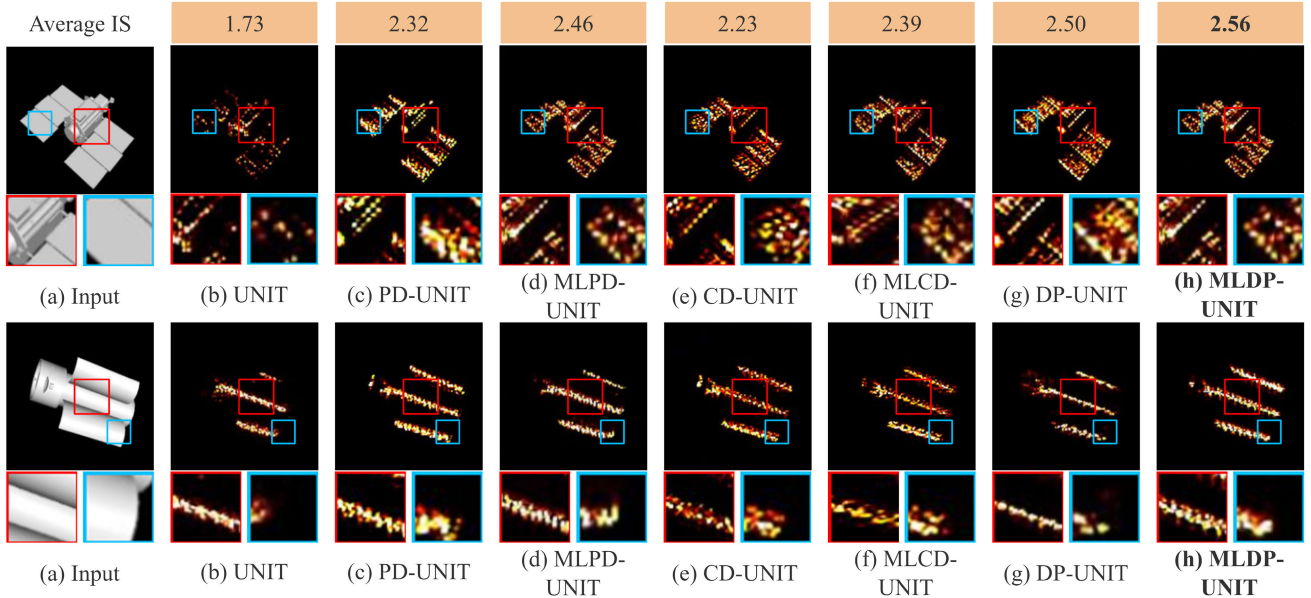


Fig. 10. The ablation results of the generated ISAR images from the original UNIT to the proposed MLDP-UNIT framework.

TABLE V  
THE TRAINING-EFFECTIVENESS RESULTS OF THE UNIT FRAMEWORK

Classifier	Generated Samples	PD-UNIT	MLPD-UNIT	CD-UNIT	MLCD-UNIT	DP-UNIT	MLDP-UNIT
VGG16	315	68.58%	70.95%	71.18%	73.14%	74.32%	<b>75.68%</b>
	630	71.08%	72.87%	72.30%	75.17%	76.86%	<b>77.03%</b>
	1260	72.64%	74.84%	73.42%	76.80%	79.31%	<b>79.43%</b>
	1890	74.37%	76.71%	75.03%	77.52%	80.57%	<b>81.52%</b>
ResNet18	315	61.35%	62.16%	62.03%	64.19%	64.93%	<b>66.05%</b>
	630	63.78%	63.51%	64.92%	67.75%	66.89%	<b>69.07%</b>
	1260	65.88%	65.54%	66.89%	68.92%	68.91%	<b>71.27%</b>
	1890	66.70%	66.98%	67.96%	71.01%	70.41%	<b>73.31%</b>

We validate the performance with/without each module in terms of visualization results, IS, and training-effectiveness. Fig. 9 and Fig. 10 present the visualization results of the ablation experiments for MLDP-CycleGAN and MLDP-UNIT. It is apparent that without the PD module, the scattering distribution features will experience a visualized performance drop. Meanwhile, somewhat counterintuitively, the ML scheme always leads to a significant improvements on the scattering distribution features. This view is echoed by the IS results listed in Table IV, as the models with ML always gain higher IS than without it. It can be seen that the PD module provides better increments on IS than CD module, and ML scheme significantly improves the IS at all cases. This suggested that the PD module does retain the visualization features in terms of the scattering distribution while the CD module tends to improve the identifying feature for better training effectiveness.

In light of this, Table III and V present the ablation results of training-effectiveness on VGG-16 and ResNet18. It is straightforward that CD module brings significantly better improvements on classification accuracy, and ML scheme still offers significant lifts (around 2%) on all cases. We note that, even the lowest case that individually applied PD module, the tested models still gain better results than the original one.

The ablation experiment shows that (i) the proposed physical domain prior mainly improves the visual-authentic in terms

TABLE VI  
THE TIME-CONSUMING RESULTS OF DIFFERENT MODELS

Model	Training time	Testing time	Parameters
CycleGAN	4.73(hours)	0.1649(s)	$4.612 \times 10^7$
AGCycleGAN	7.32(hours)	0.2309(s)	$4.183 \times 10^7$
MLDP-CycleGAN	8.05(hours)	0.1709(s)	$4.612 \times 10^7$
UNIT	4.26(hours)	0.1040(s)	$1.077 \times 10^7$
MUNIT	4.58(hours)	0.1054(s)	$1.030 \times 10^7$
SA-MUNIT	4.93(hours)	0.1065(s)	$1.030 \times 10^7$
MLDP-UNIT	6.67(hours)	0.1072(s)	$1.077 \times 10^7$

of better scattering distribution features; (ii) the classification domain prior ensures the satisfactory training-effectiveness of the generated samples; (iii) the meta-learning scheme plays a fatal rule that significantly improves the performance in the aspects of learning both of the PD and CD priors, as well as allowing the whole model learning effectively with a limited number of training samples.

4) *Time Consuming Experiments:* Table VI displays the training times for the proposed MLDP-CycleGAN and MLDP-UNIT, as well as their vanilla counterparts. The time-consuming results show that the training time of the proposed models is slightly longer due to the incorporation of the MLDP block. However, it is noted that the computational complexity and the runtime of the proposed methods are similar with the existing models, which verifies that the proposed MLDP

block only plays a role in the training process of the proposed models and does not significantly affect the inference of the test models.

## VII. CONCLUSION

This paper strives to generate ISAR images from the optical counterparts, trying to solve a fatal bottleneck in satellite classification tasks: the lack of the visual-authentic and training-effective ISAR samples for training. For the first time, a meta-learning based domain prior is proposed to model the implicit features, including the scattering distribution from ISAR physical domain and classification identifying features from task-driven domain, in ISAR images. The proposed MLDP is applied to the CycleGAN and UNIT framework to realize an authentic and effective translation from the optical domain to the ISAR domain, where a meta-learning based training scheme is applied to endow a few-shot learning capacity for limited training data via accumulating the mutual knowledge of domain priors across different samples. Extensive simulations prove their better visual-authenticity and the training-effectiveness of the generated ISAR images.

## REFERENCES

- [1] S. Zhao, Y. Luo, T. Zhang, W. Guo, and Z. Zhang, “A feature decomposition-based method for automatic ship detection crossing different satellite SAR images,” *IEEE Trans. Geosci. Remote Sens.*, vol. 60, 2022, Art. no. 5234015.
- [2] S. Zhao, Z. Zhang, T. Zhang, W. Guo, and Y. Luo, “Transferable SAR image classification crossing different satellites under open set condition,” *IEEE Geosci. Remote Sens. Lett.*, vol. 19, 2022, Art. no. 4506005.
- [3] W. Zhao, R. Chellappa, P. J. Phillips, and A. Rosenfeld, “Face recognition: A literature survey,” *ACM Comput. Surv.*, vol. 35, no. 4, pp. 399–458, 2003.
- [4] D. Gray and H. Tao, “Viewpoint invariant pedestrian recognition with an ensemble of localized features,” in *Proc. Eur. Conf. Comput. Vis.* Cham, Switzerland: Springer, 2008, pp. 262–275.
- [5] G. Dong and H. Liu, “Global receptive-based neural network for target recognition in SAR images,” *IEEE Trans. Cybern.*, vol. 51, no. 4, pp. 1954–1967, Apr. 2021.
- [6] B. Xue and N. Tong, “Real-world ISAR object recognition using deep multimodal relation learning,” *IEEE Trans. Cybern.*, vol. 50, no. 10, pp. 4256–4267, Oct. 2020.
- [7] R. Xue, X. Bai, and F. Zhou, “SAISAR-net: A robust sequential adjustment ISAR image classification network,” *IEEE Trans. Geosci. Remote Sens.*, vol. 60, 2022, Art. no. 5214715.
- [8] S. Zhao, Y. Luo, T. Zhang, W. Guo, and Z. Zhang, “Active learning SAR image classification method crossing different imaging platforms,” *IEEE Geosci. Remote Sens. Lett.*, vol. 19, 2022, Art. no. 4514105.
- [9] P. Shamsolmoali, M. Zareapoor, S. Das, S. García, E. Granger, and J. Yang, “GEN: Generative equivariant networks for diverse image-to-image translation,” *IEEE Trans. Cybern.*, vol. 53, no. 2, pp. 874–886, Feb. 2023.
- [10] A. Hertzmann, C. E. Jacobs, N. Oliver, B. Curless, and D. H. Salesin, “Image analogies,” in *Proc. 28th Annu. Conf. Comput. Graph. Interact. Techn.*, Aug. 2001, pp. 327–340.
- [11] J. Zhang, J. Zhou, and X. Lu, “Feature-guided SAR-to-optical image translation,” *IEEE Access*, vol. 8, pp. 70925–70937, 2020.
- [12] X. Huang and S. Belongie, “Arbitrary style transfer in real-time with adaptive instance normalization,” in *Proc. IEEE Int. Conf. Comput. Vis. (ICCV)*, Oct. 2017, pp. 1510–1519.
- [13] P. Isola, J.-Y. Zhu, T. Zhou, and A. A. Efros, “Image-to-image translation with conditional adversarial networks,” in *Proc. IEEE Conf. Comput. Vis. Pattern Recognit.*, Jul. 2017, pp. 1125–1134.
- [14] J.-Y. Zhu, T. Park, P. Isola, and A. A. Efros, “Unpaired image-to-image translation using cycle-consistent adversarial networks,” in *Proc. IEEE Int. Conf. Comput. Vis.*, Oct. 2017, pp. 2223–2232.
- [15] W. Xu, C. Long, R. Wang, and G. Wang, “DRB-GAN: A dynamic ResBlock generative adversarial network for artistic style transfer,” in *Proc. IEEE/CVF Int. Conf. Comput. Vis.*, Oct. 2021, pp. 6383–6392.
- [16] Y. Choi, M. Choi, M. Kim, J.-W. Ha, S. Kim, and J. Choo, “StarGAN: Unified generative adversarial networks for multi-domain image-to-image translation,” in *Proc. IEEE Conf. Comput. Vis. Pattern Recognit.*, Oct. 2018, pp. 8789–8797.
- [17] Y. Choi, Y. Uh, J. Yoo, and J.-W. Ha, “StarGAN v2: Diverse image synthesis for multiple domains,” in *Proc. IEEE/CVF Conf. Comput. Vis. Pattern Recognit. (CVPR)*, Jun. 2020, pp. 8185–8194.
- [18] X. Huang, M.-Y. Liu, S. Belongie, and J. Kautz, “Multimodal unsupervised image-to-image translation,” in *Proc. Eur. Conf. Comput. Vis. (ECCV)*, 2018, pp. 172–189.
- [19] H.-Y. Lee et al., “DRIT++: Diverse image-to-image translation via disentangled representations,” *Int. J. Comput. Vis.*, vol. 128, nos. 10–11, pp. 2402–2417, Nov. 2020.
- [20] I. Goodfellow et al., “Generative adversarial nets,” in *Proc. Adv. Neural Inf. Process. Syst.*, vol. 27, 2014, pp. 1–9.
- [21] M. Arjovsky, S. Chintala, and L. Bottou, “Wasserstein generative adversarial networks,” in *Proc. Int. Conf. Mach. Learn.*, 2017, pp. 214–223.
- [22] S. Li, Z. Yu, M. Xiang, and D. Mandic, “Reciprocal GAN through characteristic functions (RCF-GAN),” *IEEE Trans. Pattern Anal. Mach. Intell.*, vol. 45, no. 2, pp. 2246–2263, Feb. 2023.
- [23] D. G. Lowe, “Distinctive image features from scale-invariant keypoints,” *Int. J. Comput. Vis.*, vol. 60, no. 2, pp. 91–110, Nov. 2004.
- [24] Z. Wang, W. Liu, Y. Wang, and B. Liu, “Agcyclegan: Attention-guided cyclegan for single underwater image restoration,” in *Proc. IEEE Int. Conf. Acoust., Speech Signal Process. (ICASSP)*, May 2022, pp. 2779–2783.
- [25] J. Chen, L. Wang, R. Feng, P. Liu, W. Han, and X. Chen, “CycleGAN-STF: Spatiotemporal fusion via CycleGAN-based image generation,” *IEEE Trans. Geosci. Remote Sens.*, vol. 59, no. 7, pp. 5851–5865, Jul. 2021.
- [26] N. Efremova, M. E. A. Seddik, and E. Erten, “Soil moisture estimation using Sentinel-1/2 imagery coupled with CycleGAN for time-series gap filling,” *IEEE Trans. Geosci. Remote Sens.*, vol. 60, 2022, Art. no. 4705111.
- [27] J. Song, J.-H. Jeong, D.-S. Park, H.-H. Kim, D.-C. Seo, and J. C. Ye, “Unsupervised denoising for satellite imagery using wavelet directional CycleGAN,” *IEEE Trans. Geosci. Remote Sens.*, vol. 59, no. 8, pp. 6823–6839, Aug. 2021.
- [28] M.-Y. Liu, T. Breuel, and J. Kautz, “Unsupervised image-to-image translation networks,” in *Proc. Adv. Neural Inf. Process. Syst.*, vol. 30, 2017, pp. 1–9.
- [29] T. Kang and K. H. Lee, “Unsupervised image-to-image translation with self-attention networks,” in *Proc. IEEE Int. Conf. Big Data Smart Comput. (BigComp)*, Feb. 2020, pp. 102–108.
- [30] M. Mirza and S. Osindero, “Conditional generative adversarial nets,” 2014, *arXiv:1411.1784*.
- [31] H. Liu, Z. Wan, W. Huang, Y. Song, X. Han, and J. Liao, “PD-GAN: Probabilistic diverse GAN for image inpainting,” in *Proc. IEEE/CVF Conf. Comput. Vis. Pattern Recognit.*, Jun. 2021, pp. 9371–9381.
- [32] Z. Yi, H. Zhang, P. Tan, and M. Gong, “DualGAN: Unsupervised dual learning for image-to-image translation,” in *Proc. IEEE Int. Conf. Comput. Vis. (ICCV)*, Oct. 2017, pp. 2868–2876.
- [33] T. Kim, M. Cha, H. Kim, J. K. Lee, and J. Kim, “Learning to discover cross-domain relations with generative adversarial networks,” in *Proc. 34th Int. Conf. Mach. Learn.*, vol. 70, D. Precup and Y. W. Teh, Eds. Aug. 2017, pp. 1857–1865. [Online]. Available: <https://proceedings.mlr.press/v70/kim17a.html>
- [34] Q. Song, F. Xu, and Y.-Q. Jin, “SAR image representation learning with adversarial autoencoder networks,” in *Proc. IEEE Int. Geosci. Remote Sens. Symp.*, Jul. 2019, pp. 9498–9501.
- [35] Y. Sun, W. Jiang, J. Yang, and W. Li, “SAR target recognition using cGAN-based SAR-to-optical image translation,” *Remote Sens.*, vol. 14, no. 8, p. 1793, Apr. 2022.
- [36] J. Hwang, C. Yu, and Y. Shin, “SAR-to-optical image translation using SSIM and perceptual loss based cycle-consistent GAN,” in *Proc. Int. Conf. Inf. Commun. Technol. Converg. (ICTC)*, 2020, pp. 191–194.
- [37] R.-Y. Zhou, Z.-L. Yang, and F. Wang, “ISAR images generation via generative adversarial networks,” in *Proc. IEEE Int. Geosci. Remote Sens. Symp. (IGARSS)*, Jul. 2021, pp. 5267–5270.
- [38] L. Kang, Y. Luo, Q. Zhang, X.-W. Liu, and B.-S. Liang, “3-D scattering image sparse reconstruction via radar network,” *IEEE Trans. Geosci. Remote Sens.*, vol. 60, 2022, Art. no. 5100414.

- [39] L. Kang, T. Sun, Y. Luo, J. Ni, and Q. Zhang, "SAR imaging based on deep unfolded network with approximated observation," *IEEE Trans. Geosci. Remote Sens.*, vol. 60, 2022, Art. no. 5228514.
- [40] H. Zhang, J. Ni, S. Xiong, Y. Luo, and Q. Zhang, "SR-ISTA-net: Sparse representation-based deep learning approach for SAR imaging," *IEEE Geosci. Remote Sens. Lett.*, vol. 19, 2022, Art. no. 4513205.
- [41] C. Finn and S. Levine, "Meta-learning and universality: Deep representations and gradient descent can approximate any learning algorithm," 2017, *arXiv:1710.11622*.
- [42] J. Xia and D. Gunduz, "Meta-learning based beamforming design for MISO downlink," in *Proc. IEEE Int. Symp. Inf. Theory (ISIT)*, Jun. 2021, pp. 2954–2959.
- [43] J.-Y. Xia, S. Li, J.-J. Huang, Z. Yang, I. M. Jaimoukha, and D. Gündüz, "Metalearning-based alternating minimization algorithm for nonconvex optimization," *IEEE Trans. Neural Netw. Learn. Syst.*, vol. 34, no. 9, pp. 5366–5380, Sep. 2022.
- [44] Z. Yang, J.-Y. Xia, J. Luo, S. Zhang, and D. Gunduz, "A learning-aided flexible gradient descent approach to MISO beamforming," *IEEE Wireless Commun. Lett.*, vol. 11, no. 9, pp. 1895–1899, Sep. 2022.
- [45] A. Li, W. Huang, X. Lan, J. Feng, Z. Li, and L. Wang, "Boosting few-shot learning with adaptive margin loss," in *Proc. IEEE/CVF Conf. Comput. Vis. Pattern Recognit.*, Oct. 2020, pp. 12576–12584.
- [46] J. Li and M. Hu, "Continuous model adaptation using online meta-learning for smart grid application," *IEEE Trans. Neural Netw. Learn. Syst.*, vol. 32, no. 8, pp. 3633–3642, Aug. 2021.
- [47] L. Chen, B. Hu, Z.-H. Guan, L. Zhao, and X. Shen, "Multiagent meta-reinforcement learning for adaptive multipath routing optimization," *IEEE Trans. Neural Netw. Learn. Syst.*, vol. 33, no. 10, pp. 5374–5386, Oct. 2022.
- [48] S. Ravi and H. Larochelle, "Optimization as a model for few-shot learning," in *Proc. Int. Conf. Learn. Represent.*, 2016, pp. 1–11.
- [49] Q. Sun, Y. Liu, T.-S. Chua, and B. Schiele, "Meta-transfer learning for few-shot learning," in *Proc. IEEE/CVF Conf. Comput. Vis. Pattern Recognit. (CVPR)*, Jun. 2019, pp. 403–412.
- [50] Q. Sun and L. Cai, "Multi-AUV target recognition method based on GAN-meta learning," in *Proc. 5th Int. Conf. Adv. Robot. Mechatronics (ICARM)*, Dec. 2020, pp. 374–379.
- [51] R. Zhang, T. Che, Z. Ghahramani, Y. Bengio, and Y. Song, "MetaGAN: An adversarial approach to few-shot learning," in *Proc. Adv. Neural Inf. Process. Syst.*, vol. 31, 2018, pp. 1–10.
- [52] A. Sridhar, "Meta-GAN for few-shot image generation," in *Proc. ICLR Workshop Deep Generative Models Highly Structured Data*, 2022, pp. 1–11.
- [53] C. Finn, P. Abbeel, and S. Levine, "Model-agnostic meta-learning for fast adaptation of deep networks," in *Proc. Int. Conf. Mach. Learn.*, 2017, pp. 1126–1135.
- [54] A. Nichol, J. Achiam, and J. Schulman, "On first-order meta-learning algorithms," 2018, *arXiv:1803.02999*.
- [55] D. S. Tan, J. H. Soeseno, and K.-L. Hua, "Controllable and identity-aware facial attribute transformation," *IEEE Trans. Cybern.*, vol. 52, no. 6, pp. 4825–4836, Jun. 2022.
- [56] S. Zhao et al., "Emotional semantics-preserved and feature-aligned CycleGAN for visual emotion adaptation," *IEEE Trans. Cybern.*, vol. 52, no. 10, pp. 10000–10013, Oct. 2022.
- [57] J. Liu et al., "Illumination-invariant flotation froth color measuring via Wasserstein distance-based CycleGAN with structure-preserving constraint," *IEEE Trans. Cybern.*, vol. 51, no. 2, pp. 839–852, Feb. 2021.
- [58] C. Li and M. Wand, "Precomputed real-time texture synthesis with Markovian generative adversarial networks," in *Proc. Eur. Conf. Comput. Vis.* Cham, Switzerland: Springer, 2016, pp. 702–716.
- [59] D. P. Kingma and J. Ba, "Adam: A method for stochastic optimization," 2014, *arXiv:1412.6980*.
- [60] S. Barratt and R. Sharma, "A note on the inception score," 2018, *arXiv:1801.01973*.
- [61] M. J. Chong and D. Forsyth, "Effectively unbiased FID and inception score and where to find them," in *Proc. IEEE/CVF Conf. Comput. Vis. Pattern Recognit.*, Sep. 2020, pp. 6070–6079.
- [62] K. Simonyan and A. Zisserman, "Very deep convolutional networks for large-scale image recognition," 2014, *arXiv:1409.1556*.
- [63] K. He, X. Zhang, S. Ren, and J. Sun, "Deep residual learning for image recognition," in *Proc. IEEE Conf. Comput. Vis. Pattern Recognit.*, Oct. 2016, pp. 770–778.



**Huaizhang Liao** received the B.Sc. degree from the National University of Defense Technology (NUDT), Changsha, China, where he is currently pursuing the Ph.D. degree with the College of Electronic Science. His research interests include radar image generation and multimodal fusion.



**Jingyuan Xia** received the B.Sc. and M.Sc. degrees from the National University of Defense Technology (NUDT), Changsha, China, and the Ph.D. degree from Imperial College London (ICL) in 2020. He has been a Lecturer with the College of the Electronic Science, NUDT, since 2020. His current research interests include machine learning, non-convex optimization, AIGC, low level vision, and semantic learning.



**Zhixiong Yang** received the B.Sc. degree from Northeastern University, China. He is currently pursuing the M.Sc. degree with the College of Electronic Science, National University of Defense Technology. His research interests include deep learning on signal processing and image processing.



**Fulin Pan** is currently pursuing the B.Sc. degree with the National University of Defense Technology (NUDT), Changsha, China. His research interests include radar image processing and generation.



**Zhen Liu** received the M.S. and Ph.D. degrees from the National University of Defense Technology (NUDT), Changsha, China, in 2008 and 2013, respectively. He is currently a Professor with the School of Electronic Science and Engineering, NUDT. His current research interests include radar signal design, radar imaging, radar countermeasures, and compressed sensing theory.



**Yongxiang Liu** (Member, IEEE) received the B.S. and Ph.D. degrees from the National University of Defense Technology (NUDT), in 1999 and 2004, respectively. Since 2004, he has been with NUDT, where he is currently a Professor with the College of Electronic Science and Technology, conducting research on radar target recognition, time-frequency analysis, and micro-motions. He was with Imperial College London as an Academic Visitor in 2008.